J. Fluid Mech. (1994), *vol.* 267, *pp.* 109–151

Turbulent channel flow with large-amplitude velocity oscillations

By SEDAT F. TARDU,[1] GILBERT BINDER[1] AND RON F. BLACKWELDER[2]

[1] Laboratoire des Ecoulements Géophysiques et Industriels, Institut de Mécanique de Grenoble, CNRS, UJF, INPG, BP 53-X, 38041, Grenoble, Cédex-France

[2] Department of Aerospace Engineering, University of Southern California, Los Angeles, CA 90089-1191, USA

(Received 10 May 1991 and in revised form 15 October 1993)

Measurements in turbulent channel flow with forced oscillations covering a wide range of frequencies ($\omega^+ = 0.03$–0.0005) and amplitudes (10–70% of centreline velocity) are presented and discussed. Phase averages of the velocity $\langle u \rangle$ across the flow, and of the wall shear stress $\langle \tau \rangle$, as well as the turbulent fluctuations $\langle u'u' \rangle$ and $\langle \tau'\tau' \rangle$ are obtained with LDA and hot-film techniques. The time-mean quantities, except u'^2, are only slightly affected by the imposed oscillations whatever their frequency and amplitude. It is shown that the appropriate similarity parameter for the oscillating quantities $\tilde{u}$ and $\tilde{\tau}$ is the non-dimensional Stokes length l_s^+ (or the frequency $\omega^+ = 2/l_s^{+2}$). In the regime of high-frequency forcing ($l_s^+ < 10$) the oscillating flow $\tilde{u}$ and $\tilde{\tau}$ are governed by purely viscous shear forces although the time-mean flow is fully turbulent. This behaviour may be explained by the physical significance of l_s^+. At lower frequency $l_s^+ > 10$, the oscillating flow is influenced by the turbulence, in particular the amplitude of $\tilde{\tau}$ increases with respect to the Stokes amplitude and becomes proportional to l_s^+. The relative amplitude of $\langle u'u' \rangle$ and $\langle \tau'\tau' \rangle$ decreases sharply with increasing forcing frequency once $l_s^+ < 25$. This decay of the turbulence response is faster for the wall shear stress. For forcing frequencies such that $l_s^+ > 12$, $\langle u'u' \rangle$ and $\langle \tau'\tau' \rangle$ lag behind $\langle u \rangle$ and $\langle \tau \rangle$ by respectively about 75 and 130 viscous time units. These lags decrease by a factor 2 at higher forcing frequencies. It is shown that in the log layer, the turbulence modulation diffuses away from the wall with a diffusivity equal to that of the time-mean turbulence. The imposed oscillations are felt down to the small scales of the turbulence as may be evidenced from the cyclic modulation of the Taylor microscale, the skewness and the flatness factors of $\partial u'/\partial t$. The modulations of the skewness and the flatness go through a maximum around $l_s^+ = 12$.

1. Introduction

Unsteadiness imposed on a turbulent shear flow by means of time-dependent boundary conditions greatly increases its complexity because time must be added to the independent space variables and also the forcing introduces an amplitude and a timescale. Starting from a single steady flow, one type of forcing thus generates an entire two-parameter family of unsteady flows. In addition several types of forcing are generally not only possible but relevant to practical situations.

A classical example is the flow around an airfoil rendered unsteady by oscillations either of the angle of attack or of the free-stream velocity or of a combination of these two boundary conditions as on helicopter blades. Somewhat simpler situations derived

from this practical case are the unsteady flat-plate turbulent boundary layer or turbulent channel flow driven by oscillations of the free stream – or the centreline – velocity about a mean value.

The complexity of these unsteady wall flows is reflected in the difficulty in establishing which similarity parameters are physically the most relevant. Thus, for the non-dimensional frequency or Strouhal number Cousteix, Houdeville & Javelle (1977) have used $\omega X/\bar{U}_e$ (where $\omega = 2\pi f$ is the frequency of imposed oscillations, X is the distance from the leading edge of the flat plate and $\bar{U}_e$ is the time-mean free-stream velocity) to present their data. Arguing that the imposed oscillations should interact most strongly with the turbulence when their frequencies are comparable, Ramaprian & Tu (1983) have proposed $\omega\delta/\bar{u}_\tau$, where $\bar{u}_\tau$ is the friction velocity based on the time-mean wall shear stress. Since as a rough approximation $\bar{u}_\tau \propto \bar{U}_e$ and for the flat plate $\delta \propto X$, there is a relationship between these two frequency parameters.

A similarity parameter of a different kind namely $l_s^+ = l_s \bar{u}_\tau/\nu$ ($l_s = \sqrt{2\nu/\omega}$ being the thickness of the viscous Stokes layer), was introduced by Ronneberger & Ahrens (1977) and independently later by our own group (Binder & Kueny 1981). An appropriate name for this parameter could be 'Stokes–Reynolds number'. The introduction *a priori* rather surprising, of the viscous Stokes thickness was based on both studies on observations that the oscillating flow near the wall followed closely the viscous Stokes solution when the forcing frequency was high enough. It may be interesting to note that these observations pertained to quite different physical experiments since the first authors investigated air flow in a pipe with acoustic forcing and measured the oscillating wall shear stress, while our group investigated pulsed flow in a two-dimensional water channel and measured the oscillating velocity by means of LDA with the point closest to the wall at $y^+ = 3$. In order to explain the viscous behaviour of the oscillating flow at high forcing frequencies, both groups linked two facts together: one, that in this case viscosity alone diffuses the oscillating wall shear stress to a distance of the order of l_s which varies like $1/\omega^{\frac{1}{2}}$; and two, that the turbulent flow near the wall in the steady regime is dominated by viscous effects up to $y^+ \approx 12$ since below this distance the Reynolds stress is smaller than the viscous stress. Consequently, if the frequency is high enough so that $l_s^+ < 12$, the shear wave from the wall will reach the asymptotic outer values before the turbulence can play an appreciable role in the momentum transfer. This may be defined as the high-frequency regime. The oscillating flow as shown by these experiments departs progressively from the viscous Stokes solution at larger values of l_s^+.

It may easily be seen that the forcing frequency scaled with inner variables is related to l_s^+ by the simple formula $\omega^+ = 2/l_s^{+2}$. It is also interesting to note that the Strouhal number based on l_s and $\bar{u}_\tau$ is inversely proportional to l_s^+:

$$\omega l_s/\bar{u}_\tau = \sqrt{2\omega^+} = 2/l_s^+.$$

In the two experiments mentioned above which have led to the definition of l_s^+, the amplitudes of the imposed oscillations were small, 5% or less. In other experiments with larger amplitudes (Cousteix, Javalle & Houdeville 1981; Ramaprian & Tu 1983; Parikh *et al.* 1981), on the other hand, measurements could only be made in the more accessible outer regions of the shear flow and not in the lower logarithmic region or below. Yet, it is this latter region where 50% of the mean velocity variations occur and up to 100% of the change in oscillating velocity at medium or high forcing frequencies. The questions of the role of the amplitude on unsteady effects and on the relevance of the l_s^+ parameter under high-amplitude forcing could, therefore, not be answered with the existing data.

The scaling of the forcing frequency is not the only subject of controversy. Another moot point is the possible effect of the forcing on the time-mean flow. Most authors have concluded that there is no such effect (Mao & Hanratty 1986; Tardu, Binder & Blackwelder 1987; Finnicum & Hanratty 1988) even in the presence of mild adverse pressure gradients (Jarayaman, Parikh & Reynolds 1982; Brereton, Reynolds & Jarayaman 1990). The results of the Iowa group on the unsteady pipe flow (Tu & Ramaprian 1983; Ramaprian & Tu 1983), however, indicate small modifications of the time-mean characteristics when the oscillation frequency is sufficiently close to the bursting frequency or when the amplitude is large (the maximum imposed amplitude is 64% in these experiments but the corresponding imposed frequency ($l_s^+ = 40$) is quite low). The later data of the same group (Menendez & Ramaprian 1983) on a forced boundary layer show that this slight effect on the time-mean properties is concentrated in the outer layer but that the time-mean wall shear stress also decreases slightly with increasing imposed frequency. Recently, Mao & Hanratty (1991) have also reported such a decrease when the amplitude of the oscillations is large and when the imposed frequency is $\omega^+ = 0.05$. Although this question is not settled at the present time it raises the question of the possibility of manipulation of coherent structures and drag reduction via imposed oscillations. That requires sufficiently high imposed amplitudes and frequencies and the published data cover only limited range of one or both of these parameters.

The response of turbulence to unsteady forcing is a complex question but of great fundamental importance. In periodic flows it is manifested in the cyclic modulation of turbulence quantities, such as moments of fluctuations scales or structural parameters. The best documented quantity is the modulation of the wall shear stress fluctuations $\widetilde{\tau'\tau'}$ (Ramaprian & Tu 1983; Mao & Hanratty 1986; Finnicum & Hanratty 1988; Tardu & Binder 1993). These measurements show that the amplitude and phase shift of the fundamental mode of $\widetilde{\tau'\tau'}$ vary considerably with the forcing frequency. The amplitude for instance decreases sharply – by nearly an order of magnitude – and then increases when the forcing frequency is varied continuously from low quasi-steady values to very high values. Data on the modulation of the Reynolds shear stresses cover a much more restricted range of flow parameters, especially concerning the imposed amplitudes. Although some common features can now be drawn such as the increase of the phase lag of the shear stresses across the boundary layer (Ramaprian & Tu 1983; Brereton & Reynolds 1987), or the decrease of their modulation with increasing imposed frequency (Brereton *et al.* 1990; Tardu *et al.* 1987) there is still a general lack of agreement on the reaction of the near-wall turbulence.

The research reported here was specifically designed to investigate the velocity field in the logarithmic and the wall region with a wide range of imposed amplitudes and frequencies. Particular attention has been paid to studying the response of the turbulence to imposed amplitudes as high as 65% of the free-stream velocity with imposed frequencies reaching the mean bursting frequency. Detailed measurements of the wall shear stress and of the streamwise velocity modulations are reported. The effect of the imposed unsteadiness on the small and intermediate scales of the turbulence is studied through the measurements of the modulation of the zero-crossing frequency and moments of the fluctuating streamwise velocity time derivative.

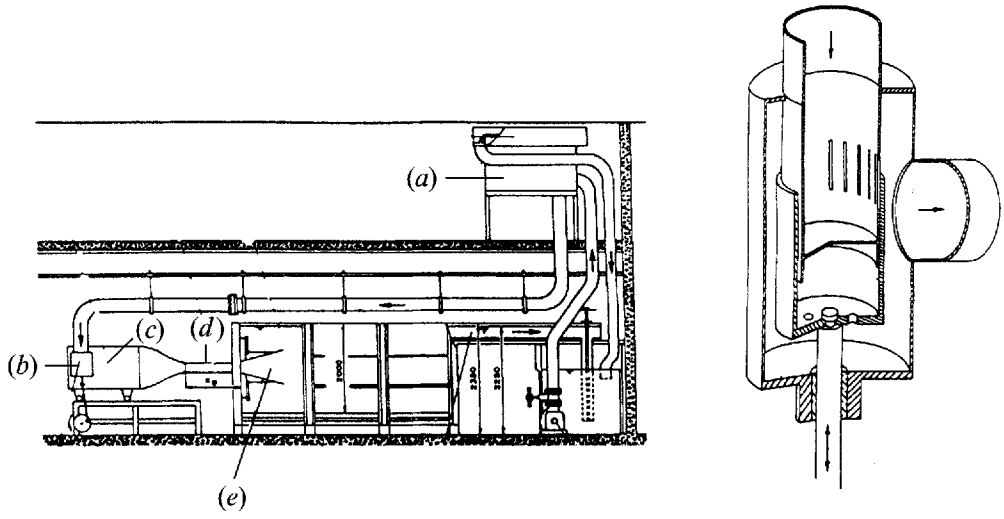

FIGURE 1. The water channel and pulsating device: (*a*) constant-head tank, (*b*) pulsating device, (*c*) setting chamber, (*d*) channel, (*e*) test section.

2. Experimental facilities

2.1. *The flow loop apparatus*

The main elements of the flow loop are: a constant-head tank with a large free surface in order to minimize variations in the total head when flow is pulsed, the pulsator, a control valve, a settling chamber with screens and a honeycomb, a converging section with a 10/1 contraction, the test channel, a large free-surface tank ($1 \times 2 \times 4.5$ m^3) and the pump (figure 1). The last metre of the channel is immersed in this tank. A divergence up to 30° can be imposed on this section to set up a time-mean pressure gradient. The return flow to the pump is via a free-surface flow in order to limit the elements of the loop subjected to large unsteady pressure forces.

The dimensions of the test channel are: width = 100 mm, length = 2600 mm, span = 1000 mm. The boundary layer at the channel entrance is tripped by tridimensional 5 mm high crenel-type roughnesses.

Oscillations in the flow rate are produced by the following device: the inflow pipe to the pulsator terminates in a cylinder having 24 longitudinal 5×200 mm slots machined in its surface (figure 1). The end of the cylinder was capped so the water had to exit through the slots. A moveable sleeve was tightly fitted around the cylinder so the sleeve covered some, all or none of the length of the slots. This apparatus was housed in a larger cylinder which collected the water exiting through the slots and allowed it to continue into the settling chamber. The oscillation frequency of the sleeve was controlled by a variable-speed motor through an eccentric bearing. The eccentricity was adjustable to control the amplitude of the oscillation. The mean flow was controlled by adjusting the length of the connecting arm between the eccentric bearing and the sleeve. These three variables were easily changed in a continuous manner and allowed great flexibility in adjusting the flow conditions. The amplitude could be varied from 0 to 80% of the mean flow and the period from 2.5 s to infinity, although the largest period studied was 132 s. The time period was repeatable within 0.1%.

The flow loop provided very stable and repeatable mean and periodic flow conditions for a given setting of the pulsator. These conditions varied by less than 0.5% from one day to another. The pulsator proved to be very convenient for the *in*

Station	l_s^+	f^+	$\bar{U}_c$ (cm s^{-1})	$a_{\tilde{uc}}$	$\bar{\tau}_{unst}/\bar{\tau}_{st}$	$(\tau'\tau')^{\frac{1}{2}}/\bar{\tau}$	$a_{\tilde{\tau'\tau'}}/a_{\tilde{\tau}}$	$\Phi_{\tilde{\tau}}-\Phi_{\tilde{uc}}$	$\Phi_{\tilde{\tau'\tau'}}-\Phi_{\tilde{uc}}$	$a_{\tilde{\tau}}/a_{\tilde{uc}}$
1	17.9	9.9345×10^{-4}	17.63	0.31	0.92	0.38	1.85	9.12	−25.10	1.82
2	17.9	9.9345×10^{-4}	17.63	0.31	0.90	0.39	1.90	7.11	−26.05	1.71
3	17.9	9.9345×10^{-4}	17.63	0.31	0.91	0.40	1.90	10.40	−24.82	1.71
4	17.9	9.9345×10^{-4}	17.63	0.31	0.96	0.40	1.78	10.54	−23.36	1.80
1	12.9	1.9069×10^{-3}	9.54	0.08	0.96	0.34	1.89	43.80	−40.70	1.62
2	12.9	1.9069×10^{-3}	9.54	0.08	0.99	0.31	1.74	30.45	−34.27	1.60
3	12.9	1.9069×10^{-3}	9.54	0.08	1.05	0.27	2.15	42.62	−57.72	1.60
4	12.9	1.9069×10^{-3}	9.54	0.08	0.97	0.30	2.31	47.25	−56.45	1.66
1	4.6	1.5043×10^{-2}	15.77	0.40	0.98	0.39	0.36	22.76	−339.55	3.61
2	4.6	1.5043×10^{-2}	15.77	0.40	1.00	0.35	0.37	18.34	−343.03	3.45
3	4.6	1.5043×10^{-2}	15.77	0.40	1.03	0.38	0.32	19.61	−341.87	3.59
4	4.6	1.5043×10^{-2}	15.77	0.40	0.94	0.41	0.31	16.75	−342.58	3.55
1	2.9	3.7849×10^{-2}	13.38	0.67	0.96	0.41	0.34	31.43	−324.4	2.24
2	2.9	3.7849×10^{-2}	13.38	0.67	1.08	0.36	0.37	23.95	−332.48	2.26
3	2.9	3.7849×10^{-2}	13.38	0.67	1.01	0.35	0.36	22.09	−330.76	2.28
4	2.9	3.7849×10^{-2}	13.38	0.67	1.09	0.39	0.38	23.98	−332.87	2.37

TABLE 1. Flow conditions at four streamwise locations for several imposed frequencies and amplitudes.

situ calibration of hot films. The effect of the periodic displacement of the wall which gives rise to a parasitic velocity oscillation seen by a fixed probe was negligible as shown in Appendix A.

2.2. *Flow characteristics*

The mean centreline velocity $\bar{U}_c$ can be varied from 0 to 50 cm s^{-1}. The corresponding maximum Reynolds number based on the half-height h of the channel is $(Re_h)_{max} = 25 \times 10^3$ and the corresponding value of Re_θ is approximately 2500. Measurements show that the flow is fully turbulent at the measuring station when $\bar{U}_c > 6$ cm s^{-1}. For most of the data presented here $\bar{U}_c = 17.5$ cm s^{-1} and $Re_h = 8500$. Even with a centreline amplitude of 64% the flow was still turbulent under static conditions when the flow rate was minimum, thus avoiding the undesirable complications which could be produced by periodic transitions. On the other hand, with $\bar{U}_c = 17.5$ cm s^{-1} the value of the friction velocity was $\bar{u}_\tau = 0.89$ cm s^{-1}, so that the inner scale $l_\nu = \nu/\bar{u}_\tau$ was $l_\nu \approx 0.126$ mm which made it possible to make LDA velocity measurements down to $y^+ = 3$ despite the large span of the channel and to explore the inner layer.

The variations of the centreline velocity in the spanwise direction were less than 2%. This was expected on account of the large 10/1 aspect ratio of the channel. The symmetry of the mean and of the periodic flow with respect to the centreplane was also checked.

Because of space limitations the channel length is only $52h$ and the measurement station was at a distance $42h$ from the entrance. This length is rather short to ensure fully developed turbulent flow despite the rather large height of the entrance trip, since this length should be about $90h$ at $Re_h = 25000$ (Comte-Bellot 1965). The development length of the turbulent flow is, however, neither uniform across the channel nor the same for different quantities: it is faster near the wall than in the core and its rate decreases with the order of the moment considered. Since the transverse gradients of the oscillating field are entirely or, at very low forcing frequencies, almost entirely confined within the inner layer, as shown by previous measurements and confirmed by present ones, the requirement on the channel length can, therefore, be relaxed without putting undue restrictions on the generality of the results. This conclusion is supported by the fact that the measured time-mean velocity and longitudinal turbulent intensity are the same at the measuring station and $6h$ further downstream and are in good agreement with previously published data. Furthermore, the time mean and periodic characteristics of the wall shear stress were measured at four stations located respectively at $x/h = 32$, 38.3, 44.6 and 50.8 from the channel entrance. The results for four typical cases are given in table 1. It is seen in these conditions with the centreline velocity of 9.54 cm s^{-1}, that the characteristics of the mean values and of the modulations of the wall shear stress and of its turbulent fluctuations are the same at these four locations within experimental accuracy. It may, therefore, be concluded that the flow is sufficiently well established at $x/h = 42$ for the type of measurements reported here.

3. Instrumentation: data acquisition and reduction

3.1. *Instrumentation*

LDA measurements

The streamwise velocity in the channel flow was measured by a one-component 25 mW laser Doppler anemometer (Binder *et al.* 1985*a*). The dimensions of the measuring volume were 0.3 and 1.5 mm ($2.3 \times 12 l_\nu$). These dimensions could be

reduced by a factor of 5 by use of a 5X-beam expander. Measurements as close as 0.25 mm $\approx 2.5 l_\nu$ (for $\bar{U}_c = 17.5$ cm s^{-1}) were then possible, but not without difficulty because the signal quality very close to the wall is poor and the sampling rate is quite small (a few samples/s).

The period of the Doppler signal was determined by a homemade counter (Tardu, Binder & Blackwelder 1986). The Doppler signal was frequency shifted with a Pockel cell in order to make measurements in reverse flow. McLaughlin & Tiederman's (1973) correction was applied in order to eliminate the statistical bias due to the proportionality between sampling rate and velocity when the processor is not saturated, as was the case here. Incidently, this can simply be done by determining the average Doppler period as well as the average Doppler frequency as shown in Appendix B.

Hot-film measurements

The wall shear stress τ was measured with Dantec 55R46 or TSI 1268 W flush-mounted hot-film probes (sensing surfaces 0.2×0.75 mm ($1.6 \times 6 l_\nu$) and 0.127×1 mm ($1 \times 8 l_\nu$) respectively). They were operated at overheat ratios between 3 and 8% with Disa 55MO1 or Dantec 56C01 constant-temperature anemometers. Bucking amplifiers or a digital to analog converter were used to suppress the DC anemometer output at zero velocity, so that the signal could be amplified before A/D conversion. This conversion was mostly performed with an Analog-Device RTI-800 board (accuracy: 11 bit+sign; 8 channels) installed in an Olivetti 240 PC computer.

The hot-film gauges were calibrated *in situ* by determining the velocity gradient at the wall with the LDA. To do this properly requires several measuring points within the viscous sublayer ($y^+ < 5$) and the precise determination of the y-position, two requirements which come up against great practical difficulties. As already mentioned above, measurements are not possible here below $y^+ = 2.5$ and they are difficult for $2.5 < y^+ < 5$, because of the low sampling rate which, combined with the high turbulence level, requires extremely long integration times (2 hours or more). The y-positions are known accurately only to within an additive y_0 because the exact position of the wall cannot be determined. In order to be able to use some points beyond $y^+ = 5$ and to reduce the uncertainty about the exact location of the wall, u_τ and y_0 are both obtained from a least-squares fit of the measured profile with the empirical relation $u^+ = 14.5 \tanh(y^+/14.5)$ for $y^+ < 14.5$. This law differs from Eckelmann's data (Eckelmann 1974; originally tabulated data kindly provided by the authors) by less than 2% over the range of y^+ from 0 to 14.5).

The mean wall shear stress determined with this method was aptly correlated by the Blasius formula: $\bar{\tau} = 0.048 Re_h^{-\frac{1}{4}} (\frac{1}{2}\rho \bar{U}_c^2)$. This empirical relation was subsequently used to determine $\bar{\tau}$ from the measurement of $\bar{U}_c$. The exponent in the heat transfer law: $E^2 = A + B\bar{\tau}^n$, where E is the output from the hot-film set, was always found to be between 0.33 and 0.35. Consequently, the theoretical value of 1/3 from the Lévêque solution consistent with the results of Spence & Brown (1968) was used (see also Appendix C). The calibration constants A and B were usually determined from five couples $(E, \bar{\tau})$.

At large amplitudes, reverse flow was encountered at the wall. Figure 2 shows the phase average of the modulation of the wall shear stress $\langle \tau \rangle$ in such a case. Pedley (1976) has shown that the response of the thermal boundary layer in reversing flow depends on the frequency parameter $\omega^* = \omega^+ (L_f^{+2} Pr)^{\frac{1}{3}} = \omega^+ Pe^{\frac{1}{3}}$, where ω^+ and L_f^+ are respectively the angular frequency and the streamwise length of the sensor in wall units, Pr is the molecular Prandtl number of the fluid and Pe is the Péclet number. In our case $\omega^+ < 0.03$ and the response of the thermal boundary layer may be considered as quasi-

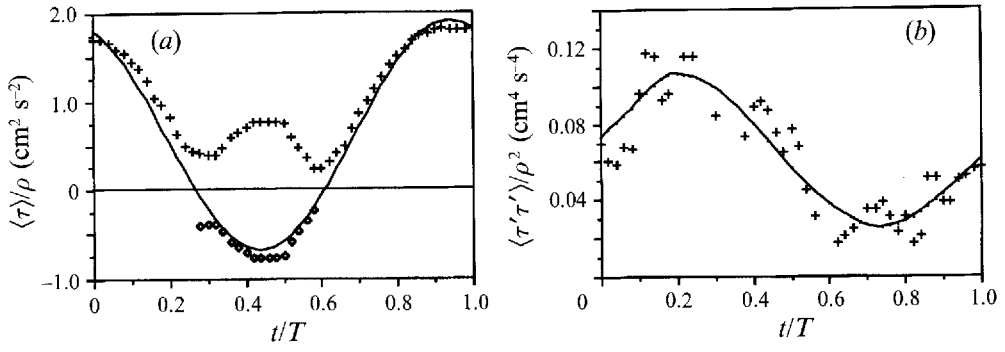

FIGURE 2. Examples of phase averages in the presence of reverse flow. $l_s^+ = 12$, $a_{\widetilde{uc}} = 70$. $\bar{U}_c = 18.5$ cm s^{-1}. (*a*) Wall shear stress $\langle\tau\rangle$; (*b*) intensity of the turbulent wall shear stress fluctuations $\langle\tau'\tau'\rangle$.

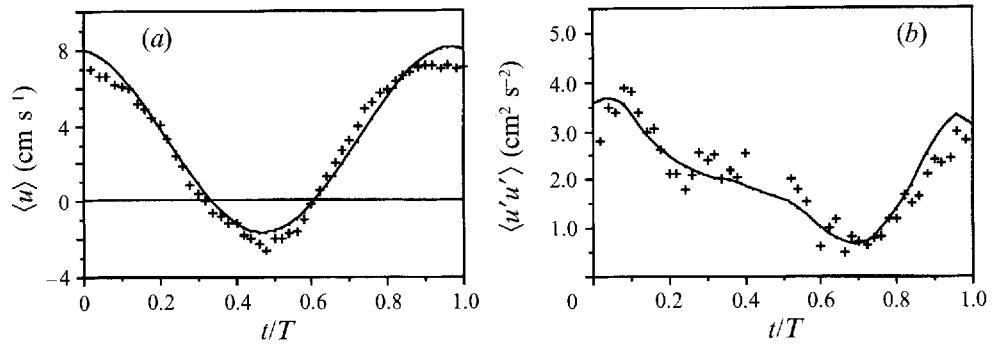

FIGURE 3. Examples of phase averages, LDA measurements: $y^+ = 4.86$, $l_s^+ = 8.1$, $\bar{U}_c = 17.5$ cm s^{-1}, $a_{\widetilde{uc}} = 0.64$. (*a*) Velocity $\langle u\rangle$, (*b*) intensity of turbulent velocity fluctuations $\langle u'u'\rangle$.

steady. Figure 2 for instance corresponds to $\omega^* = 0.04$. On the other hand when flow reversal occurs, the heat transfer rate does not reach zero because of diffusion effects. The heat transfer rate measured at $\langle\tau\rangle = 0$ is three times greater than the value given by the boundary-layer analysis of Pedley (1976) and the numerical solutions of Kaiping (1985) which neglect the axial diffusion. Since this diffusion is important in our case on account of the small value of the time-mean Péclet number $Pr\,L_f^{+2}$ a complete numerical solution of the whole thermal elliptical equation was carried out. The numerical solutions are in good agreement with the measurements (Tardu 1988; see Appendix C). Since the response of the boundary layer is quasi-steady, the film output during flow reversal has been rectified by taking the symmetry with respect to zero (figure 2; see also figure 23).

Some measurements were also performed with a single-fibre hot-film probe (model Dantec 55R11, sensing element: 70 μm = $0.6l_\nu$ in diameter and 1.25 mm = $11l_\nu$ long) mainly for the velocity time derivative and the zero-crossing frequency measurements. The calibration of this probe was done in the channel with the LDA by a least-squares fit to the relation $E^2 = A + Bu^n$; n was found to be between 0.45 and 0.5. For these measurements a 15 bit+sign Preston A/D converter was used with a sampling frequency of 500 Hz (i.e. 4.2 to $8\bar{u}_\tau^2/\nu$) after prefiltering the signal by a Krohn-Hite filter. The total duration of the record used was $2.2 \times 10^5 \nu/\bar{u}_\tau^2$.

The calibration of the hot films was checked before and after each measurement. Because of the low overheat ratio used in water, the hot-film measurements are quite

sensitive to temperature drifts. The temperature of the water was continuously monitored. In order to minimize temperature variations, the water of the flow loop is cooled by a heat exchanger supplied with tap water. In the best conditions, the temperature change was less than 0.1 °C per hour. When the integration time exceeded 15 mn, the film response was corrected for the temperature drift by assuming linear variation over the time interval.

3.2. *Data reduction*

The notation $\bar{q}$, $\tilde{q}$ and q' is used to designate respectively the time-mean, periodic and random turbulent part of the quantity q so that in established flow

$$q(y,t;T) = \bar{q}(y)+\tilde{q}(y,t/T)+q'(y,t).$$

The angle brackets designate the ensemble or phase average:

$$\langle q(y,t/T)\rangle = \bar{q}(y)+\tilde{q}(y,t/T) = \lim_{N\to\infty}\left(\sum_{i=1}^{N} q(t+iT)\right).$$

it follows that $\langle q'\rangle = 0$ and $\langle q^2\rangle = (\langle q\rangle)^2+\langle q'q'\rangle$.

The quantity $\langle q'q'\rangle$ is a function of t/T and, in keeping with the expression for $\langle q\rangle$, it is convenient to write $\langle q'q'\rangle(t/T) = \overline{q'q'}+\widetilde{q'q'}(t/T)$, where $\widetilde{q'q'}$ is the 'modulation' of the variance about the time-mean value $\overline{q'q'}$. Neither $\tilde{q}$ nor $\widetilde{q'q'}$ are necessarily pure sine functions and are most conveniently described by the amplitudes and phases of the successive terms of the Fourier series. In the present results the fundamental mode is generally dominant although higher harmonics may in some instances be substantial, especially in the turbulence modulations. An adequate description of the modulation is then given by the amplitude and phase of the fundamental mode, designated by $A_{\widetilde{()}}$ and $\Phi_{\widetilde{()}}$ where the index is the quantity under consideration, for example, $A_{\tilde{q}}$ and $\Phi_{\tilde{q}}$ or $A_{\widetilde{q'q'}}$ and $\Phi_{\widetilde{q'q'}}$. Finally the relative modulation, i.e. the amplitude of the modulation with respect to the time-mean value of the same quantity $A_{\widetilde{()}}/\overline{()}$, will be designated by a lower-case letter $a_{\widetilde{()}}$, for example $a_{\tilde{q}} = A_{\tilde{q}}/\bar{q}$ or $a_{\widetilde{q'q'}} = A_{\widetilde{q'q'}}/\overline{q'q'}$.

The phase-locked ensemble averages $\langle q\rangle$ and $\langle q'q'\rangle$ necessary to determine $\bar{q}$, $\tilde{q}(t/T)$ and $\langle q'q'\rangle(t/T)$ were obtained by dividing the cycle into bins of equal width (generally 50) and the desired quantity was averaged in each bin. The beginning of each cycle was provided by a pulse from a photoelectric cell triggered by the pulsator. Errors on long time averages due to slow drifts in the forcing period were thus avoided.

Examples of phase averages are shown on figure 3. Fourier analysis was applied to these phase averages in the following form:

$$\langle q\rangle = \bar{q}+A_{\tilde{q}}\cos(\omega t+\Phi_{\tilde{q}})+\sum_{n=2}^{\infty} A_{\tilde{q}n}\cos(n\omega t+\Phi_{\tilde{q}n}),$$

and similarly for $\langle q'q'\rangle$. The coefficients of the first ten modes were systematically computed and recorded.

Statistical convergence of the phase averages was checked by inspecting the data points. The truncated Fourier series limited to the first or to the first three modes was drawn through the data points as shown on the example of figure 3. Poor convergence was revealed by large scatter of the data points with respect to the smooth Fourier series. In most cases an integration time of $10^5\nu/\bar{u}_\tau^2$ ($\approx$ 15–25 mn) was sufficient to ensure satisfactory statistical convergence of the phase averages.

	l_s^+	$a_{\widetilde{uc}}$
■	8.1	0.64
◆	8.1	0.30
+	16	0.64
▲	23	0.64
×	34	0.64
□	Steady flow	
■	Eckelmann (1972), steady channel flow	

TABLE 2. Symbols used on figures 4, 5, 8, 13, 14 for measurements made using LDA

	$\bar{U}_c$ (cm s^{-1})	$a_{\widetilde{uc}}$	T (s)
△	28.5	0.13	2.6–33
×	19.0	0.19	3–31
◆	30.0	0.27	2.6–61
◇	30.0	0.17	2.6–61
□	30.0	0.10	2.6–15
■	18.5	0.70	4–132
▲	16–26	0.60	6
○	Houdeville *et al.* (1984)		
●	Menendez & Ramaprian (1983)		
□	Mao & Hanratty (1986)		

TABLE 3. Symbols used on figures 6, 7, 11, 15 for measurements made using a flush-mounted hot-film gauge

4. Results and discussion

The complete profiles of $\bar{u}$, $\tilde{u}$ and $\widetilde{u'u'}$ of unsteady flows forced at four different frequencies such that $l_s^+ = 8.1$, 16, 23, 34 (see table 2) and with a centreline amplitude of 64% have been measured with LDA. Flows with high-frequency forcing $l_s^+ = 8.1$ but with a centreline amplitude of 30% have also been investigated.

The properties of $\bar{\tau}$, $\tilde{\tau}$ and $\widetilde{\tau'\tau'}$ measured with the flush-mounted hot-film gauge have been determined by varying the period of the imposed oscillations from 2.6 to 132 s, i.e. $l_s^+ = 8.1$ to 64, for centreline amplitudes between 10 to 70% (table 3). Since the frequency parameter $l_s^+ = (2/\omega\nu)^{\frac{1}{2}}\bar{u}_\tau$ also depends upon $\bar{u}_\tau$, which is roughly proportional to the centreline velocity, measurements have also been performed with different centreline velocities. In one case with 60% centreline amplitude, the velocity was varied between 16 and 26 cm s^{-1}.

4.1. *The time-mean characteristics*

4.1.1. *The mean velocity*

The mean velocity distributions $\bar{u}^+(y^+)$ are shown on figure 4 for steady and unsteady flow conditions. The time-mean unsteady velocities are compared with the mean velocities at the same y^+ position for the same value of $\bar{U}_c$. The steady flow measurements compare well with Eckelmann's (1974) data at a similar Reynolds number. The closest measurement point to the wall is at $y^+ = 4$ and the flow field is explored from the viscous sublayer into the logarithmic layer. The unsteady profiles obtained with two different amplitudes and four different frequencies are shown on the same figure. Clearly there is no effect of the imposed unsteadiness on the time-mean

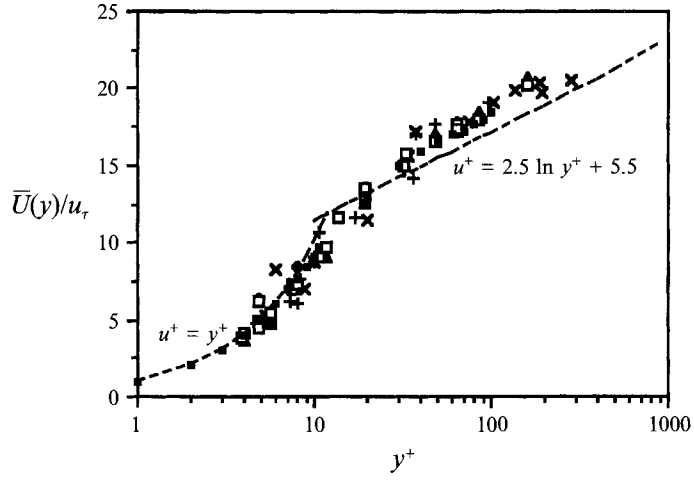

FIGURE 4. Mean velocity profiles in steady and unsteady flow. For legend see table 2.

velocity profiles despite the large forced amplitudes. These results are significant since for $l_s^+ = 8.1$ and $a_{\widetilde{uc}} = 0.64$, the amplitude of the velocity oscillations becomes greater than the local mean velocity near the wall and periodic flow reversal occurs. They confirm the findings of Karlsson (1959), Cousteix *et al.* (1981) and Binder & Kueny (1981) obtained, however, for smaller values of the imposed amplitude.

Mizushina, Maruyama & Shiozaki (1973) and Mizushina, Maruyama & Hipasawa (1975) and Ramaprian & Tu (1983) have suggested that the insensitivity of the mean flow to imposed oscillations may only be true at low amplitudes and low frequencies, i.e. at frequencies significantly below the bursting frequency. The bursting frequency reported by Blackwelder & Haritonidis (1984) is $f_b^+ = 0.0035$ and the value given more recently by Coughran & Bogard (1987) is $f_b^+ = 0.0062$. Since $f^+ = (\pi l_s^{+2})^{-1}$, it is seen that the highest frequency of the present experiments is $f^+ = 0.005$ which is close to the values given above and, yet, the mean flow remains unaltered even for imposed amplitudes as high as $0.64\overline{U}_c$.

The oscillating flow may interact with the mean flow directly via the oscillating part of the Reynolds stress $\widetilde{uv}$, or indirectly via $\overline{u'v'}$ since the Reynolds equation for the mean flow is

$$u_j \frac{\partial \overline{u_i}}{\partial x_j} = -\frac{1}{\rho}\frac{\partial \tilde{p}}{\partial x_i} + \frac{\partial}{\partial x_j}\left[\tfrac{1}{2}\nu\left(\frac{\partial \overline{u_i}}{\partial x_j} + \frac{\partial \overline{u_j}}{\partial x_i}\right) - \overline{u_i' u_j'} - \overline{\widetilde{u_i}\widetilde{u_j}}\right].$$

The results presented in this subsection suggest that $\widetilde{uv}$ is negligible and that the mean Reynolds stress is unaltered by imposed velocity oscillations. Although an order-of-magnitude analysis must be used with caution in unsteady flows because of the phase shifts between the oscillating terms, it may still be noted that in an unsteady boundary layer without an adverse pressure gradient $\partial\tilde{u}/\partial x \approx 0$ and by continuity $\tilde{v} \approx 0$ so that $\widetilde{uv} \approx 0$ and this is *a fortiori* true in channel flow.

4.1.2. *The longitudinal turbulent intensity*

The dominating impression from figure 5, which shows profiles of the time-mean longitudinal turbulent intensity $(\overline{u'u'})^{\frac{1}{2}}/\overline{u}_\tau$, is that the unsteadiness has no dramatic effect on this quantity even in these cases of large-amplitude forcing, and the classical profiles are found in steady and unsteady flows with a maximum at $y^+ = 12$ (Coles

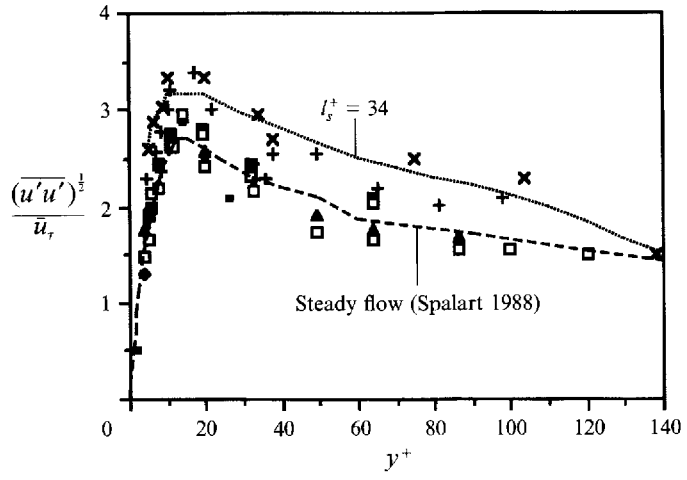

FIGURE 5. Mean turbulent intensity profiles in steady and unsteady flow. For legend see table 2.

1978). The observed differences between the various flows on this graph must be viewed while remembering that the measured $(\overline{u'u'})^{\frac{1}{2}}/\bar{u}_\tau$ *vs.* y^+ distributions in steady flow vary somewhat with Reynolds number (Wei & Willmarth 1989) and from one experiment to another. Notwithstanding these differences between steady flows, there is a systematic increase in the turbulent intensity in the forced flows at low frequency: thus in the case $l_s^+ = 34$, the maximum value at approximately $y^+ = 12$ is about 15% higher, and further away from the wall the intensity is about 30% higher than in steady flow, as also compared with the direct simulation data of steady turbulent boundary layer at $Re_\theta = 670$ reported by Spalart (1988).

These results do not agree with the earlier measurements of Mizushina *et al.* (1975) who found an increase of the mean turbulent intensity at high forcing frequencies which they interpreted as a sort of resonance between the turbulence and the imposed oscillations in these conditions. Such trends were also found by Tu & Ramaprian (1983, p. 43; their data corresponding to $l_s^+ = 14$ and $a_{\widetilde{uc}} = 0.15$), who adopted a similar point of view.

The production term in the transport equation of $\overline{u'u'}$ is

$$\overline{-\langle u'v'\rangle \frac{\partial \langle u\rangle}{\partial y}} = -\overline{u'v'}\frac{\partial \bar{u}}{\partial y} - \overline{\widetilde{u'v'}\frac{\partial \tilde{u}}{\partial y}}$$

since by definition $\tilde{u} = 0$ and $\overline{\widetilde{u'v'}} = 0$. The relative insensitivity of the $\overline{u'u'}$-profiles indicates that the production by the interaction with the oscillating velocity gradient $\overline{\widetilde{u'v'}\,\partial\tilde{u}/\partial y}$ is small compared with $\overline{u'v'}\,\partial\bar{u}/\partial y$ unless $\overline{u'v'}$ is itself affected by the imposed unsteadiness or the other mechanisms, namely turbulent transport and dissipation, exactly counterbalance the increased production, which is an unlikely eventuality. The production of the oscillating terms could only be appreciable if the terms $\widetilde{u'v'}$ and $\partial\tilde{u}/\partial y$ were comparable in amplitude with the corresponding mean values in overlapping intervals and if they were nearly in phase. The absence of effects on the mean turbulent intensity at high forcing frequencies, say $l_s^+ \leqslant 8$, observed here is consistent with the measurements of the oscillating velocity $\tilde{u}$ analysed in the next section, which show that $\partial\tilde{u}/\partial y$ is essentially confined in a layer of thickness l_s^+ in this case. The contribution of the oscillating flow $\overline{\widetilde{u'v'}\,\partial\tilde{u}/\partial y}$ to the total turbulent production $-\overline{\langle u'v'\rangle\,\partial\langle u\rangle/\partial y}$ could, therefore, be locally appreciable only in the unlikely situation where the modulation

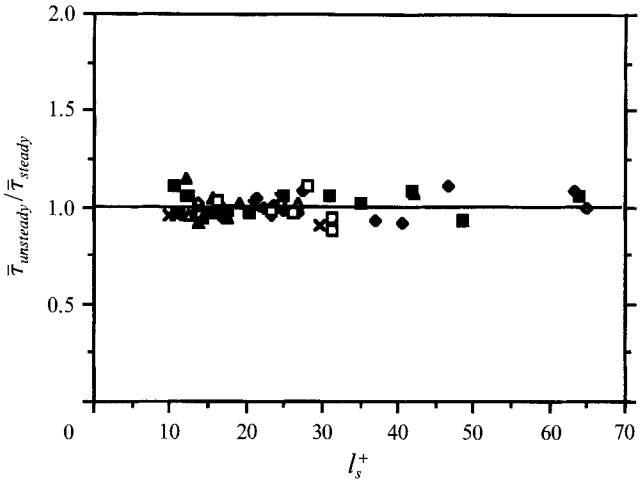

FIGURE 6. Ratio of unsteady to steady time mean wall shear stress. For legend see table 3.

$-\widetilde{u'v'}$ could reach large values between $y^+ = 0$ and l_s^+ and, even then, there would be an excess production in a thin layer so that its contribution to the production integrated over the whole boundary layer would still be small. Conversely, when l_s^+ and the forcing amplitude are large enough, as in the present case for $l_s^+ = 34$, the oscillating flow can appreciably contribute to the total production and raise the turbulence level as observed here.

4.1.3. *The wall shear stress*

Figure 6 shows the ratio of the unsteady to the steady mean wall shear stress corresponding to the same mean velocity *vs.* l_s^+. These measurements were performed by changing the imposed frequency by a factor of 40 and the imposed amplitude by a factor of 7, but also by modifying the mean Reynolds number while the oscillation period was kept constant, in order to prove the validity of the similitude parameter l_s^+. It is seen that within a scatter of $+14\%$ and -9% the time-mean wall shear stress is not affected by the oscillations. This is *a priori* surprising because of the nonlinear relationship between the wall shear stress and the centreline velocity in turbulent flow. It will be shown below that, at low frequencies ($l_s^+ > 20$), the wall shear stress is in phase with the centreline velocity as may be expected in the quasi-steady flow (qs). The Blasius formula may then be assumed to hold at any instant of the cycle so that

$$\langle \tau \rangle_{qs} = \tfrac{1}{2} C(\langle U_c \rangle h/\nu)^{-\frac{1}{4}} \rho \langle U_c \rangle^2.$$

If $\bar{\tau}_{steady}$ is the shear stress corresponding to the mean velocity,

$$\bar{\tau}_{steady} = C\left(\frac{\bar{U}_c h}{\nu}\right)^{-\frac{1}{4}} \tfrac{1}{2} \rho \bar{U}_c^2.$$

We write

$$\langle U_c \rangle = \bar{U}_c(1 + a_{\widetilde{uc}} \cos \omega t) \quad \text{and} \quad \langle \tau \rangle_{qs} = \bar{\tau}_{steady}(1 + a_{\widetilde{\tau(qs)}} \cos \omega t).$$

Then expanding and retaining two terms yields

$$\langle \tau \rangle_{qs} = \bar{\tau}_{steady}(1 + \tfrac{7}{4} a_{\widetilde{uc}} \cos \omega t + \tfrac{21}{32} a_{\widetilde{uc}}^2 \cos^2 \omega t).$$

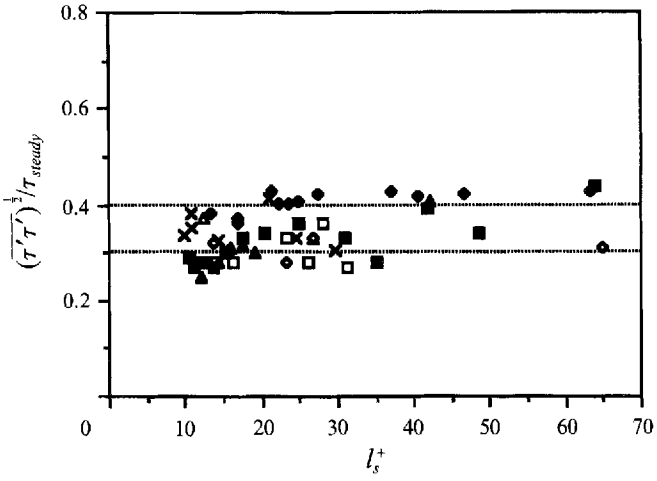

FIGURE 7. Time-mean r.m.s. values of the turbulent wall shear stress fluctuations (for legend see table 3).

Hence $$\overline{\tau}_{qs} = \overline{\tau}_{steady}(1 + \tfrac{21}{64}a_{uc}^2).$$

For the largest amplitude $a_{\widetilde{uc}} = 0.7$ the result is: $\overline{\tau}_{qs} = 1.16\overline{\tau}_{steady}$.

The predicted increase in $\overline{\tau}$ due to nonlinear effects is also at most 16% in the present experiments and is nearly buried in the experimental scatter. One may note the tendency of the solid squares, corresponding to 70% amplitude, to lie on the average above the value one.

From the present measurements, it is not possible to conclude that there is a drag-reducing (or increasing) effect of roughly 9% or less. The drag reduction reported by Mao & Hanratty (1991) was observed with an imposed frequency ($l_s^+ = 6$) which is significantly larger than the maximum investigated here. Although such a tendency was also recently observed by us for $l_s^+ < 6$ (Tardu & Binder 1993, figure 2*a*) one should be careful in drawing immediate conclusions owing to the limited confidence in the indirect measurements and the treatment of reversing flows.

4.1.4. *The turbulent wall shear stress fluctuations*

The time mean r.m.s. of the turbulent fluctuations of the unsteady wall shear stress is plotted on figure 7. $(\overline{\tau'\tau'})^{\frac{1}{2}}$ is 0.26 to 0.45 times $\overline{\tau}_{steady}$ with a mean value of 0.34. In spite of the difficulty in making such measurements – for instance, values as low as 0.06 have been reported in the literature (Chambers, Murphy & McEligot 1982) – the results agree well with the steady values of Sandborn (1979). The mean value of 0.34 compares well with the 0.36 found from the direct simulation data of Kim, Moin & Moser (1987). No trend was observed as the frequency varied suggesting that the r.m.s. value of the fluctuating shear stress $(\overline{\tau'\tau'})^{\frac{1}{2}}$ is unaffected, as was found approximately for $\overline{u'u'}$.

These results are remarkable when it is considered that in some regions the amplitude of the oscillations was greater than 100% of the local mean flow, so that reverse flow occurred over 25% of the cycle. At these large forcing amplitudes $A_{\widetilde{uc}}/\overline{u}_\tau = 15$ and the energy in the periodic flow is at least 25 times greater than in the turbulent fluctuations. In spite of this there is no apparent change in the statistics of the mean flow, implying that the mean flow is essentially decoupled from the large amplitude oscillations.

4.2. *The characteristics of the cyclic variation*

All the oscillating quantities $\tilde{u}$, $\tilde{\tau}$, $\widetilde{u'u'}$ and $\widetilde{\tau'\tau'}$ are functions of t/T. The full representation of these time functions for all the points across the flow and all the values of the forcing amplitude and forcing frequency would be very cumbersome. Therefore, as mentioned earlier only the amplitude and phase of the fundamental Fourier mode are retained. The description of an entire function by only two numbers is acceptable in as much as the higher modes are comparatively small. This is always the case here even though the forcing amplitudes were large enough to generate nonlinear effects. Conversely, in order to make a fair judgement on the importance of the oscillating flow data it should be kept in mind that every point on the amplitude and phase plots summarizes an entire time-dependent phase-average curve.

4.2.1. *Amplitude and phase shifts of the velocity oscillations*

The results concerning the oscillating part of the velocity field are presented as a function of $y_s = y/l_s$. This scaling serves to emphasize coincidences with and departures of the oscillating velocity from the viscous Stokes solution. In unsteady turbulent boundary layers, the usual lengthscales of l_ν or δ would only be appropriate for the similarity of quasi-steady properties of the flow. The parameter $l_s^+ = l_s/l_\nu$, however, indicates how far the viscous Stokes layer would penetrate into the turbulent boundary layer if it were unaffected by the turbulence.

The profiles of the amplitude and of the phase shift of the fundamental mode of the velocity oscillations $\tilde{u}$ for the five different forcing conditions are presented in figures 8(*a*) and 8(*b*). Only the fundamental is considered because it contains most of the energy of the oscillations at all y-positions. The first harmonic, for instance, is typically less than 5% of the fundamental.

The most striking result on these figures is that for the highest frequency investigated, corresponding to $l_s^+ = 8.1$, both the amplitude and the phase shift are close to the viscous Stokes solution. Thus, a phase shift of $+33°$ has been measured at $y_s = 0.6$, while the Stokes solution for this point gives $+31°$ and the extrapolation of the phase-shift to $y_s = 0$ falls close to $+45°$ which is characteristic of the Stokes solution.

The explanation of the behaviour of the oscillating velocity $\tilde{u}$ in the high-frequency regime lies in the fact that within a distance $y^+ = 12$ from the wall viscous effects dominate over turbulence effects. In steady turbulent flow, for instance, the ratio of viscous to turbulent shear stress is larger than one up to $y^+ = 12$. Now, the purely viscous Stokes layer has a thickness of roughly $2l_s$, since at a distance l_s from the wall the amplitude and phase of $\tilde{u}$ are respectively 85% and 70% of the values at infinity and since beyond $2l_s$ the velocity oscillates essentially as a plug flow in which the oscillating vorticity is zero. Thus, when $l_s^+ \leqslant 6$, $\tilde{u}$ reaches the asymptotic outer values under the (nearly) sole effect of molecular viscosity before the turbulence can effectively enhance the diffusion of vorticity. An equivalent argument is to consider that, if molecular viscosity should diffuse the oscillating vorticity to a distance less than $12l_\nu$ during the period T, it is necessary that

$$(12l_\nu)^2/\nu < T),$$

i.e. $l_s^+ < 6.8$. This condition is close to the one given above.

Thus, viscous diffusion alone governs the removal of unsteady vorticity from the wall for frequencies such that $l_s^+ \leqslant 6$. Turbulence does not participate in the diffusion, because at distances from the wall where turbulent diffusion becomes important there

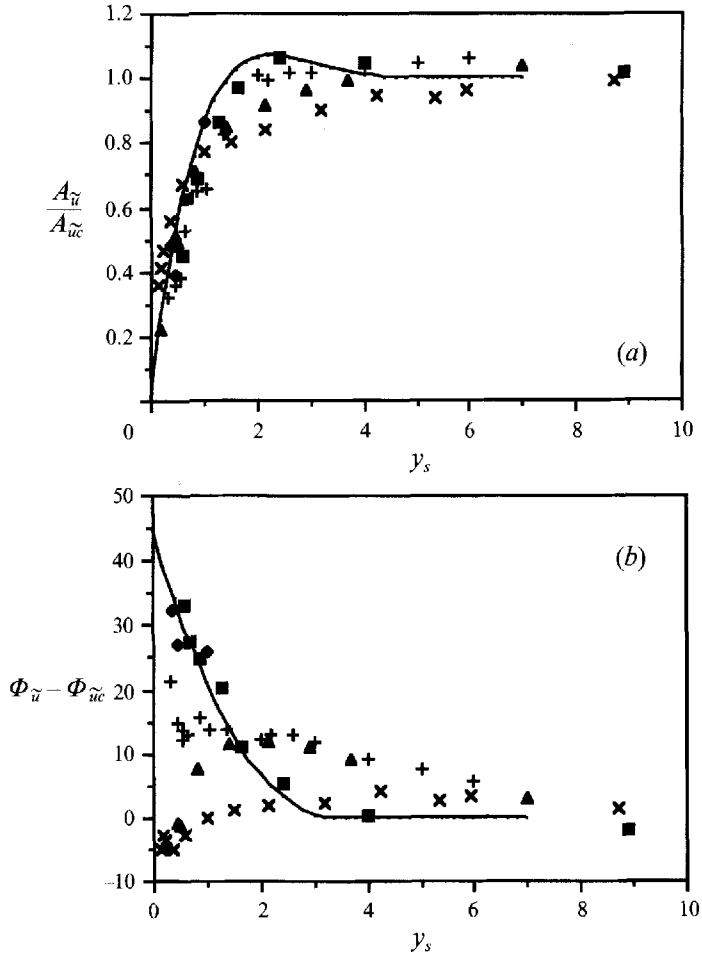

FIGURE 8. Evolution of the periodic streamwise velocity oscillations with distance from the wall. (*a*) Amplitude profiles: ——, viscous Stokes solution. (For legend see table 2.) (*b*) Phase shift profiles with respect to the centreline velocity oscillations.

is no vorticity left to diffuse. Considering the qualitative nature of these arguments, it is clear that the inferred upper limit of l_s^+ of 6 to 7 for purely viscous oscillating flow is only approximate. The present results which show that the viscous behaviour is well verified for $l_s^+ = 8.1$ as well as other observations presented below indicate that this upper limit is somewhat higher, close to 10.

It follows from the same arguments that the oscillating velocity should progressively depart from the viscous Stokes solution when l_s^+ is increased beyond this critical value. This is well born out by the results on figures 8(*a*) and 8(*b*) and it is particularly clear for the phase shift which appears as a more sensitive parameter than the amplitude. It is seen that the maximum phase lead near the wall progressively decreases with increasing values of l_s^+ and becomes negative, i.e. a phase lag, at the two lowest frequencies corresponding to $l_s^+ = 23$ and 34. In these two flows the phase shift with respect to the centreline velocity is always less than 10°. This represents less than 3% of the cycle and stresses the need for great care in the measurements.

Although the changes in the amplitude profiles of $\tilde{u}$ are not dramatic in this representation, it is clear that at the lowest frequency for $l_s^+ = 34$, the profile is both

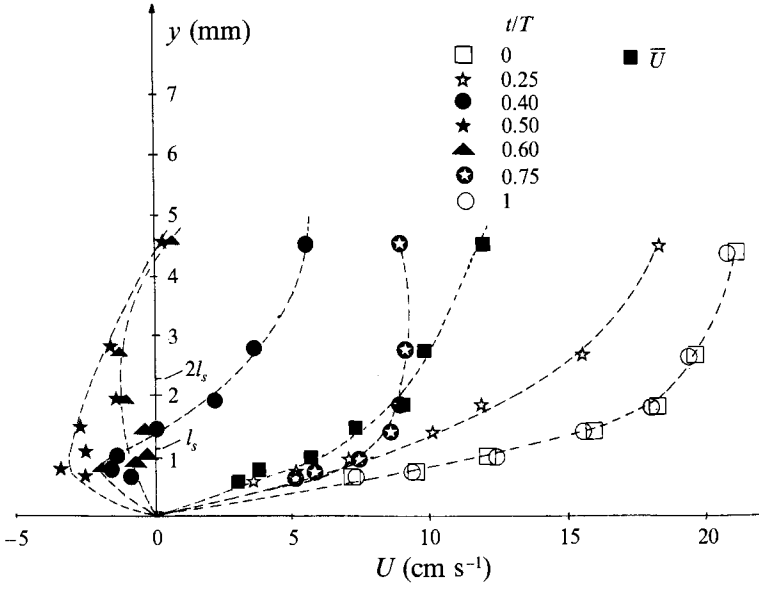

FIGURE 9. Instantaneous velocity profiles in the presence of reverse flow. $\bar{U}_c = 16.9$ cm s^{-1}, $a_{\widetilde{uc}} = 0.64$; $l_s^+ = 8.1$.

steeper near the wall and thicker than the Stokes profile. This is in keeping with the effect of turbulence in steady flows: it increases the shear stress in the wall region and, therefore, the viscous stress at the wall, and at the same time the large scales diffuse the vorticity to greater distances into the flow. It is seen that for $l_s^+ = 34$, there is oscillating vorticity to a distance from the wall of approximately $y^+ = y_s l_s^+ = 8 \times 34 = 272$, while at the highest frequency of the experiments it extends only to $y^+ = 2 \times 8 = 16$.

Even though the flows in the present experiments were forced with a centreline velocity amplitude of 64%, the results on the oscillating velocity agree surprisingly well with the earlier measurements (Binder & Kueny 1981) performed in flows with small oscillation amplitudes ($a_{\widetilde{uc}} = 5$ or 3%). On figures 8(*a*) and 8(*b*) there are also a few points corresponding to a forcing with $a_{\widetilde{uc}} = 30\%$ and $l_s^+ = 8.1$. These points are close to those of the flow forced at the same frequency and at larger amplitude. It may, therefore, be concluded that, in the case of channel flow, nonlinear effects due to the forcing amplitude are small up to centreline amplitudes as large as 64%. This is not exactly what might be expected at a first glance, especially if it is remembered that at the higher frequencies the local amplitudes become larger than 100% near the wall.

Attention is finally drawn to the fact that the amplitudes in the immediate neighbourhood of the wall are slightly below the Stokes curve at the highest frequencies for $l_s^+ = 8.1$ and 16. This is an apparently paradoxical result since it means that the oscillating wall shear stress is less than the purely viscous value in turbulent channel flow! Experimental inaccuracies were first suspected, especially since near-wall measurements are particularly difficult. These points were, therefore, checked with care and this result was confirmed. This point will be further discussed in the section on the oscillations of the wall shear stress in §4.2.3.

4.2.2. *Observation of reverse flow*

One of the more interesting consequences of the Stokes-type flow is that at sufficiently large amplitude, reverse flow without separation can occur near the wall over part of the oscillation cycle. Reverse flow appears at a given point when $\langle u \rangle < 0$

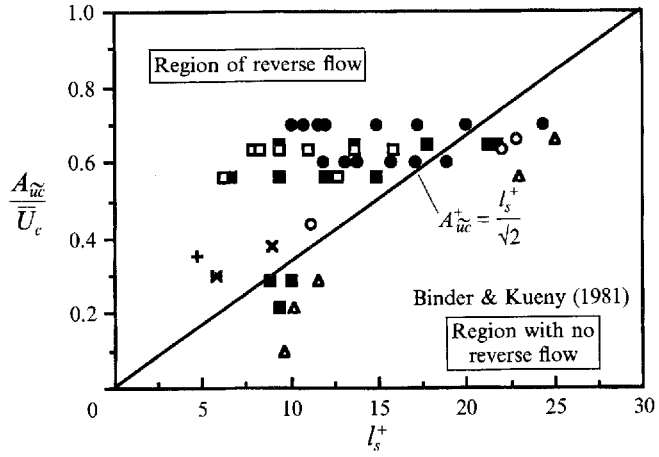

FIGURE 10. Observations of reverse flow compared with the Binder–Kueny criterion, given by the straight line: ●, Hot film; ■, Visualizations; □, LDA; ○, $y_s = 1$; $u = 0$; ⋈, $y_s = 0.5$; $u = 0$; △, Visualizations: no reverse flow; +, Karlsson (1959); ×, Jarayaman *et al.* (1982)

which implies that $A_{\tilde{u}} > \bar{u}$. The instantaneous profiles corresponding to $l_s^+ = 8.1$ and $a_{\widetilde{uc}} = 0.64$ shown on figure 9, demonstrate the existence of negative velocities in some parts of the oscillation cycle.

In the near-wall region where both $A_{\tilde{u}}$ and $\bar{u}$ vary linearly with y, the condition $A_{\tilde{u}} > \bar{u}$ is equivalent to $A_{\partial u/\partial y} > \partial\bar{u}/\partial y$ and therefore equivalent to $A_{\bar{\tau}} > \bar{\tau}$. If it is further assumed that the oscillations follow the Stokes solution, i.e. $A_{\bar{\tau}} = \sqrt{2}\,\mu A_{uc}/l_s$, the condition for reverse flow is then

$$\sqrt{2}\,A_{\widetilde{uc}}/l_s > \bar{u}_\tau^2/\nu,$$

i.e. $A_{\widetilde{uc}}/\bar{u}_\tau > l_s^+/\sqrt{2}$ or $A^+_{\widetilde{uc}} > l_s^+/\sqrt{2}$.

This simple criterion first derived by Binder & Kueny (1981) combines the amplitude and the frequency of the oscillation in one formula and shows that the occurrence of reverse flow will depend upon both parameters.

The validity of this criterion for flow reversal is amply confirmed by the experimental observations plotted on figure 10. These have been made with three different techniques: a frequency-shifted LDA, flush-mounted hot-films, and flow visualizations with a hydrogen bubble wire either parallel or perpendicular to the wall as well as with dye injected through a slot in the wall. It is seen that the values lying above the line $A_{uc}/\bar{u}_\tau > l_s^+/\sqrt{2}$ experience reverse flow as predicted by the above criterion up to $l_s^+ = 20$. For larger values of l_s^+, the line of separation between flows with and flows without reversal lies below the straight line of the criterion which means that flow reversal will occur for lower amplitudes than those predicted for a given l_s^+. This is consistent with the steepening of the velocity amplitude gradient at the wall produced by the turbulence at the larger values of l_s^+, which is clearly demonstrated by the measurements of the oscillating wall shear stress discussed in the next section.

The earlier observations of reverse flow of Karlsson (1959) and Jarayaman *et al.* (1982) also plotted on the figure are in agreement with the criterion. The observations of the latter authors are particularly interesting because they were made in a mild adverse pressure gradient and thus prove indirectly that Stokes flow may still occur in such circumstances. We have recently made similar observations in a small-angle (2.4°) diffuser.

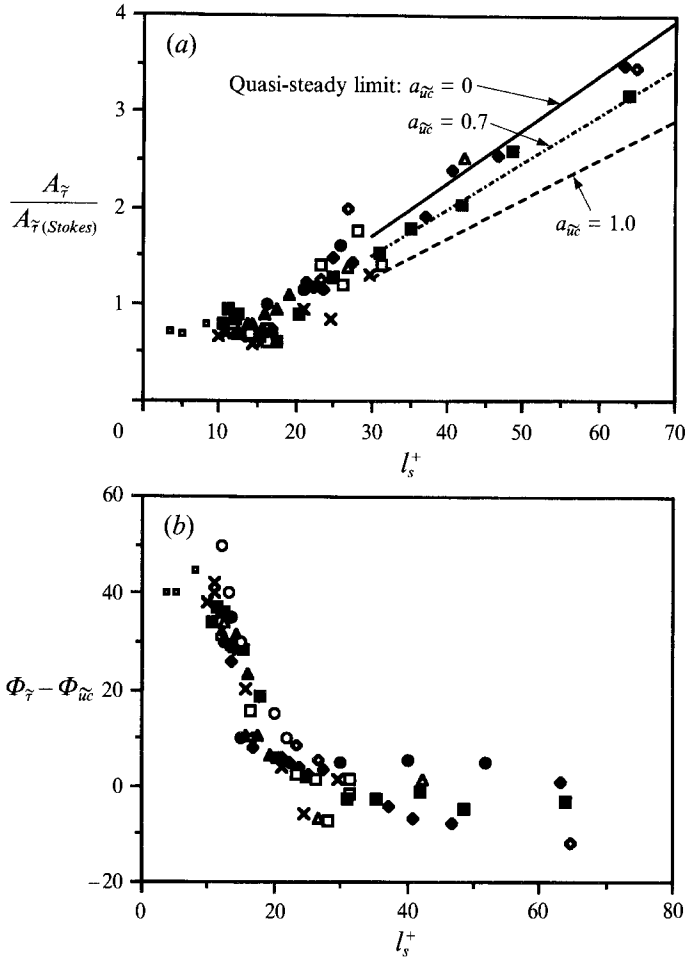

FIGURE 11. Oscillations of the wall shear stress *vs.* frequency parameter l_s^+ (for legend see table 3). (*a*) Amplitude normalized by the Stokes value. (*b*) Phase shift with respect to the centreline velocity oscillations.

The flow reversal of the three visual observations on figure 10 which do not conform with the criterion was probably due to turbulent fluctuations near the minimum velocity. On the other hand, the linear part of $A_{\tilde{u}}^+$ may extend further into the outer layer than $\overline{u}^+$ which gives an area of negative velocity in the internal part of the flow and this is not foreseeable with the criterion given above.

4.2.3. *The oscillation of the wall shear stress*

The evolutions of the amplitude $A_{\tilde{\tau}}$ and of the phase shift $\Phi_{\tilde{\tau}} - \Phi_{\widetilde{uc}}$ of the oscillating wall shear stress are plotted *vs.* l_s^+ on figures 11(*a*) and 11(*b*).

The amplitude is non-dimensionalized with the amplitude of the viscous Stokes stress at the same frequency, i.e. $A_{\tilde{\tau}(Stokes)} = \sqrt{2}\mu A_{\widetilde{uc}}/l_s$. The ratio $A_{\tilde{\tau}}/A_{\tilde{\tau}(Stokes)}$ thus involves entirely distinct quantities which, moreover, are measured with different techniques: $A_{\tilde{\tau}}$ is measured with the wall hot-film gauge while $A_{\tilde{\tau}(Stokes)}$ is determined from the frequency and the centreline amplitude measured by LDA. The data on figure 11 were obtained by varying the frequency and the amplitude of the imposed oscillations respectively by a factor 50 and 7, and by changing the shear velocity via the

centreline velocity by a factor 1.6. It should be stressed that l_s^+ is more sensitive to changes in $\bar{u}_\tau$, i.e. to the Reynolds number, than in ω since it is directly proportional to $\bar{u}_\tau$ but only inversely proportional to the square root of ω. The fairly good collapse of the data points for both the amplitude and phase shift on single curves is, therefore, physically significant and supports the claim that l_s^+ is the appropriate similarity parameter for the near-wall unsteady flow.

At the higher frequencies, $l_s^+ < 10$, the amplitude of τ is close to the Stokes value and the frequency shift with respect to the outer velocity oscillation approaches 45° as predicted by the Stokes solution. These wall shear stress measurements also clearly confirm the conclusion drawn from the velocity measurements, namely that in the high-frequency regime the oscillating flow ignores the existence of the turbulence.

A neat confirmation of this result was recently provided by measurements of the acoustic impedance of pneumotachographs to forced oscillations. The method of forced oscillations is a promising non-intrusive technique for the physiological investigation of the lung, which does not require the cooperation of the patient who can breathe freely through a supply tube during the test. The method was developed under the restriction that the flow in the supply tube was laminar. Louis & Isabey (1990) have recently shown that this severe restriction may be relaxed and that the method is still applicable when the flow is turbulent provided that the forcing frequency is high enough to make l_s^+ smaller than 10. Their measurements show that the impedance in turbulent flow departs from the viscous values only once $l_s^+ > 10$.

It is further observed that both the amplitude and the phase shift of $\langle\tau\rangle$ move rapidly away from the viscous limit as soon as $l_s^+ > 10$. When $l_s^+ = 20$ the phase shift is nearly zero and the amplitude is close to the quasi-steady turbulent value as discussed below.

The phase-shift data of Menendez & Ramaprian (1983), Mao & Hanratty (1986) and Houdeville, Jullien & Cousteix (1984) (taken in a flat-plate boundary layer) are also shown on figure 11(*b*). The agreement with the present measurements is quite satisfactory when it is kept in mind that 10° is less than 3 % of the cycle. The phase shift *vs.* l_s^+ curve seems thus to have a universal character. It is remarkable that this curve does not depend on the amplitude of the oscillations.

Houdeville *et al.* (1984) encountered serious difficulties in measuring the wall shear stress oscillations with the flush-mounted hot film in air owing to the parasitic heat transfer through the substrate which produces a considerable reduction in the frequency response. In order to minimize this unwanted transfer these authors developed a probe where a flush-mounted hot-film is placed above a small cavity. The results of these authors quoted above were obtained with such a probe. Our results obtained with a similar probe in water are shown on figure 12. The phase shifts measured in this way were systematically higher than those obtained with the flush-mounted film. For instance, at the lowest l_s^+, phase shifts as high as 60° were obtained (figure 12*b*). A small change in the wall configuration may thus have a noticeable effect on the probe response.

Close inspection of the high-frequency data of figure 11(*a*) reveals that the amplitude ratio is systematically smaller than one at the highest frequencies. There is actually a dip in the curve around $l_s^+ = 15$. This surprising result of a shear stress smaller than the purely viscous value – consistent with the observations made earlier on the gradient of the amplitude of the oscillating velocity near the wall – was noted before by Ronneberger & Ahrens (1977) in their investigation of pipe flow subjected to small-amplitude acoustic forcing. The dip in the amplitude ratio near $l_s^+ = 11$ is unmistakable in their plot owing to the smaller scatter in their data. These authors attempt to explain

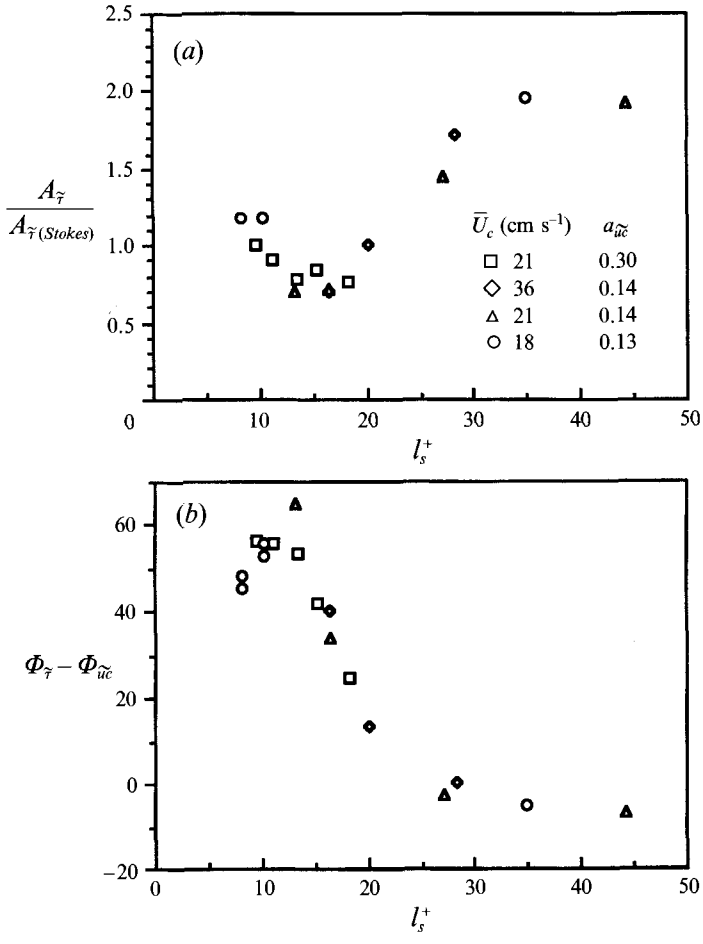

FIGURE 12. Oscillations of the wall shear stress measured with the Houdeville–Cousteix gauge. (*a*) amplitude, (*b*) phase shift.

this behaviour with a model which takes the effective viscosity (the molecular plus the eddy viscosity) with distance from the wall into account. Because of this increase in effective viscosity, the outward diffusing shear wave is partly reflected back towards the wall by the buffer layer and the resulting shear wave is weaker if the interference is destructive. This accounts in a qualitative way for the minimum in the $A_{\tilde{\tau}}/A_{\tilde{\tau}(Stokes)}$ data. Indeed, if $l_s^+ < 10$ then the shear wave is already strongly attenuated when it reaches the buffer layer and the reflected wave is weak. On the other hand, when $l_s^+ > 15$, the shear wave is enhanced by turbulent diffusion and $A_{\tilde{\tau}} > A_{\tilde{\tau}(Stokes)}$. Ronneberger & Ahrens (1977) find fair quantitative agreement with their data by assuming a rigid wall at $y^+ = 15$, i.e. total reflection at this location. With the more realistic assumption of an effective viscosity where the eddy viscosity is based on the Prandtl mixing length and the formula of van Driest, the computed $A_{\tilde{\tau}}/A_{\tilde{\tau}(Stokes)}$ curve unfortunately does not display a minimum. One may speculate that a time-dependent eddy viscosity which could in particular be phase shifted with respect to the shear could perhaps account better for these observations.

The shear variation was also found to be smaller than the Stokes value at high frequency in the data reported by Mao & Hanratty (1986) as it is seen in figure 11(*a*).

These authors have developed a relaxation model whereby the flow close to the wall sees an effective pressure gradient which introduces a lag between the imposed velocity oscillations and the change of scale in the viscous wall region. This method predicts quite well the decrease of $A_{\tilde{\tau}}/A_{\tilde{\tau}(Stokes)}$ in the high-frequency regime. This decrease was however not confirmed by the subsequent measurements of Finnicum & Hanratty (1988). The authors explained these differences by a possible pipe diameter effect. The hydraulic equivalent diameter of the channel used in this study is indeed very close to the pipe diameter of Mao & Hanratty (1986) but significantly larger than in Finnicum & Hanratty's experiments.

The amplitude of the oscillating shear stress increases monotonically with l_s^+ and is larger than the Stokes value when $l_s^+ > 20$. In the present experiments values nearly three times larger than the viscous stress at the corresponding frequency have been measured. As pointed out earlier, this is due to turbulent diffusion once the oscillating layer is thick enough to penetrate into the region where turbulent diffusion dominates molecular transport.

From the relationships derived for the quasi-steady limit in §4.1 one obtains for the amplitude of the fundamental mode

$$\frac{A_{\tilde{\tau}(qs)}}{A_{\tilde{\tau}(Stokes)}} = \frac{7}{4\sqrt{2}} \frac{1}{1+\frac{21}{64}a_{\widetilde{uc}}^2} \frac{\bar{u}_\tau}{\bar{U}_c} l_s^+.$$

Since in the present experiments $\bar{u}_\tau/\bar{U}_c = 1/22$, it follows that

$$\frac{A_{\tilde{\tau}(qs)}}{A_{\tilde{\tau}(Stokes)}} = \frac{0.056}{1+\frac{21}{64}a_{\widetilde{uc}}^2} l_s^+.$$

The lines for $a_{\widetilde{uc}} \to 0$, and $a_{\widetilde{uc}} = 0.7, 1$ are drawn on figure 11(*a*). It is seen that the data are in satisfactory agreement with this simple relationship: the points for the smaller amplitudes are close to the line calculated with $a_{\widetilde{uc}} = 0$ while the points for the 70% amplitude case fall – but for one exception – on the line corresponding to $a_{\widetilde{uc}} = 0.7$.

4.2.4. *The modulation of the longitudinal turbulent intensity*

The amplitude profiles of the modulation $\widetilde{u'u'}$ of the longitudinal turbulent intensity for the four flows investigated are plotted in three ways in order to illustrate different features.

The variations in the absolute level of $A_{\widetilde{u'u'}}$ across the flow and with the oscillation frequency ($a_{\widetilde{uc}} = 0.64$ in all four cases) are most clearly shown by normalizing the amplitude with the constant mean shear velocity as on figure 13(*a*). This representation also facilitates comparison with the mean turbulent intensity of figure 5 and it is seen that amplitude profiles are similar to the mean profiles with a peak around $y^+ = 12$–15.

The most important observation is that the higher the oscillation frequency, the smaller the modulation of the turbulence is. Thus, the maximum value of $A_{\widetilde{u'u'}}$ for the highest frequency, $l_s^+ = 8.1$ is only half the value for $l_s^+ = 24$ or 34 and it tends to zero more rapidly. At the highest frequency $A_{\widetilde{u'u'}}$ is zero as soon as $y^+ > 60$ while at the lowest frequency $l_s^+ = 34$, $A_{\widetilde{u'u'}}$ is still about $5\bar{u}_\tau^2$ at $y^+ = 100$. This behaviour is amply confirmed by the modulation of the turbulent shear stress that will be discussed in the next section.

The interpretation of this observation is that at the higher frequencies the turbulence can no longer follow the imposed oscillation and has an attenuated response. This

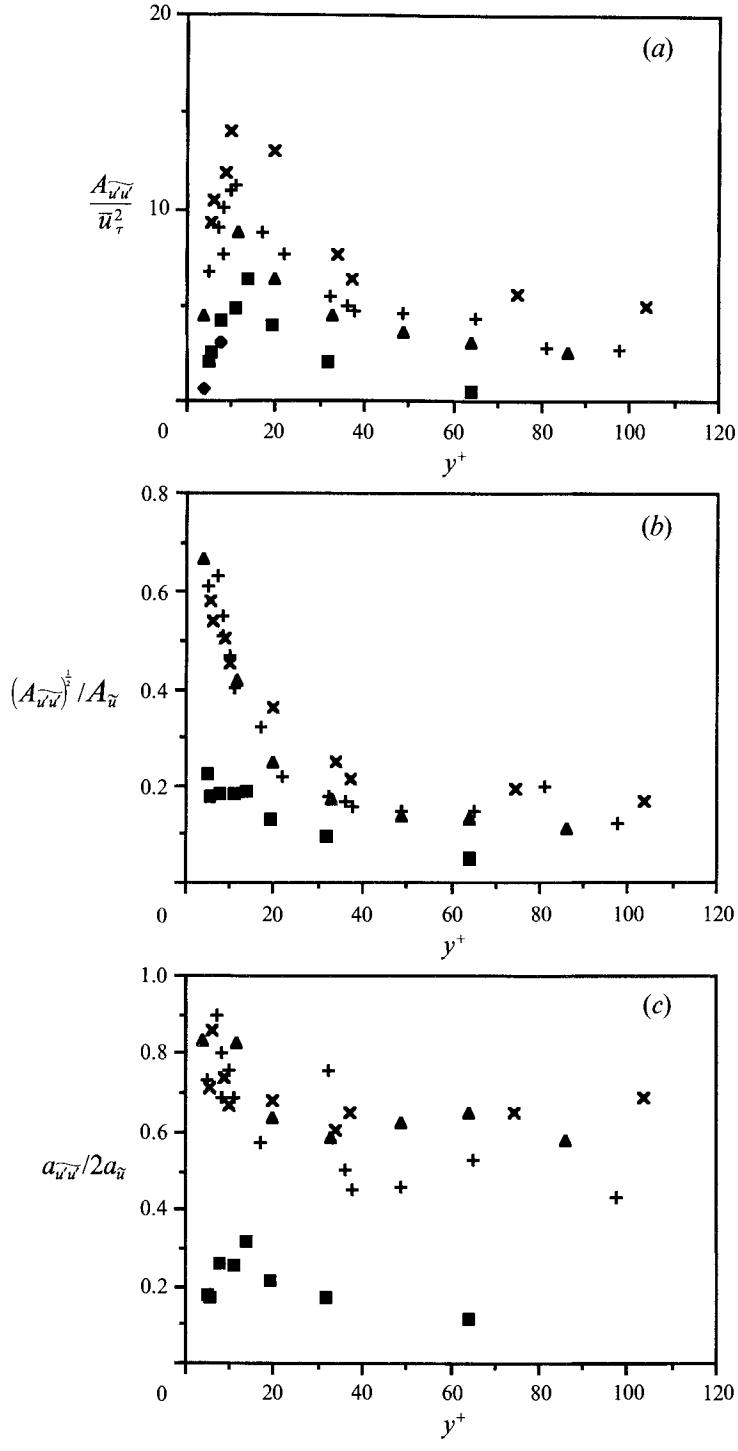

FIGURE 13. Amplitude profiles of the modulation of the longitudinal turbulent intensity. For legend see table 2. (*a*) Values scaled with constant time-mean shear velocity. (*b*) Intensity with respect to local velocity oscillations. (*c*) Ratio of relative amplitudes of turbulent fluctuations and local velocity oscillations.

contradicts some earlier ideas according to which the interaction of the imposed oscillations with the turbulence should be most intense when their frequencies are comparable, as happens when resonance occurs (Mizushina *et al.* 1973; Ramaprian & Tu 1983). The most energetic turbulent eddies near the wall have a frequency $\omega^+ \approx 0.1$ according to the spectra measured at $y^+ = 15$ by Compte-Bellot (1965) while the frequency of the imposed oscillations in the $l_s^+ = 8.1$ case is only 0.03. Clearly the response of the turbulence is already attenuated at frequencies lower than that energy-containing eddies.

The modulation of the local relative turbulent intensity $(A_{\widetilde{u'u'}})^{\frac{1}{2}}/A_{\tilde{u}}$ of figure 13(*b*) is reminiscent of the ratio $(\overline{u'^2})^{\frac{1}{2}}/\bar{u}_\tau$ of the mean values. It is seen that the attenuation of the modulation of the turbulence in the high-frequency case is brought out even more clearly in this representation since near the wall there is a factor 3 difference between the high-frequency values and those of the three other cases. The good collapse of the points of these latter flows up to $y^+ = 20$ is also noteworthy. There is, hence, a sharp change in the turbulence response when l_s^+ decreases below the value 16.

Comparison of the modulation of turbulent intensity with the time-mean value would be misleading in the representation of figure 13(*b*). Indeed, in the quasi-steady limit $\langle u'u' \rangle / \langle u \rangle^2$ should be a function of $\langle y^+ \rangle$ only. Indeed the law of the wall $\bar{u}^+ = f(y^+)$ and $(\overline{u'^2})^{\frac{1}{2}}/\bar{u}_\tau = g(y^+)$ in steady flow yields

$$\frac{\overline{u'^2}}{\bar{u}^2} = \frac{g(y^+)}{f^2(y^+)} = F(y^+).$$

In the quasi-steady limit one should have then

$$\left(\frac{\langle u'u' \rangle}{\langle u \rangle^2}\right)_{(qs)} = F(\langle y^+ \rangle),$$

where $\langle y^+ \rangle = \langle u_\tau \rangle y/\nu$. Now F is a slowly varying function of y^+ (Eckelmann 1974) so that for small-amplitude forcing one should have

$$\left(\frac{\langle u'u' \rangle}{\langle u \rangle^2}\right)_{(qs)} \approx \text{const.}$$

Hence

$$\frac{\overline{u'u'}(1 + \widetilde{u'u'}/\overline{u'u'})}{\bar{u}^2(1 + 2\tilde{u}/\bar{u})} \approx \text{const.}$$

i.e.

$$\frac{\widetilde{u'u'}}{\overline{u'u'}} = 2\frac{\tilde{u}}{\bar{u}},$$

which means that the turbulence is in phase with the velocity and that

$$\frac{A_{\widetilde{u'u'}}}{\overline{u'u'}} = 2\frac{A_{\tilde{u}}}{\bar{u}} \quad \text{or} \quad a_{\widetilde{u'u'}} = 2a_{\tilde{u}}.$$

In order to compare the turbulent intensities of the periodic and of the mean flow, one should thus consider $A_{\widetilde{u'u'}}/A_{\tilde{u}}$ and $\overline{u'u'}/\bar{u}^2$ or equivalently the relative amplitudes $a_{\widetilde{u'u'}}$ and $a_{\tilde{u}}$ and not the ratio with the r.m.s. values. The plot of $a_{\widetilde{u'u'}}/2a_{\tilde{u}}$ (figure 13*c*) shows again the sharp difference between high-frequency case and the others: the turbulence drops at least by a factor 1 and by as much as a factor 4 throughout the flow in the high-frequency case. It is observed that $a_{\widetilde{u'u'}}/2a_{\tilde{u}}$ is closest to one in the

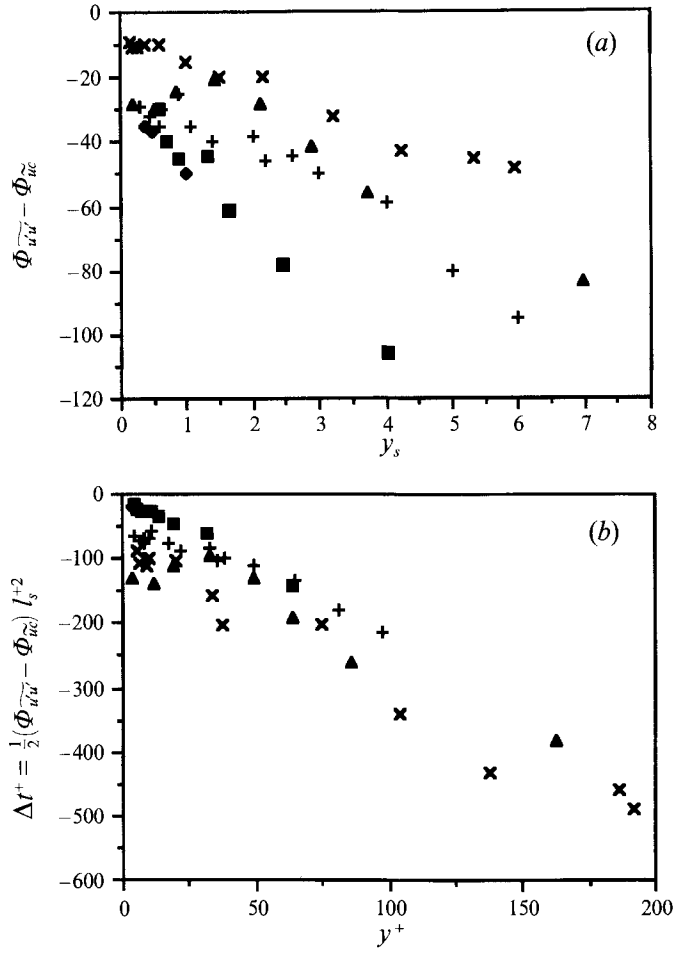

FIGURE 14. Variations of the phase of the turbulent velocity fluctuation modulation with distance from the wall. For legend see table 2. (*a*) Phase shift with respect to the centreline oscillations. (*b*) Time lag.

neighbourhood of the wall but does not quite reach this value. This is not surprising considering that one is the quasi-steady *small-amplitude* limit and that 64% forcing amplitude of these flows is certainly not small. One may, on the contrary, be rather surprised that the value $a_{\widetilde{u'u'}}/2a_{\tilde{u}}$ is so close to one for such a large-amplitude forcing, in other words that the turbulence response does not saturate more rapidly with the forcing amplitude.

The phase shift profiles of $\langle u'u' \rangle$ with respect to the velocity oscillation $\langle U_c \rangle$, drawn on figure 14(*a*), show that the modulation of the turbulence always lags behind the modulation of the velocity as in a relation between cause and effect. It is clear from this figure that the lag decreases with l_s^+ at a fixed y_s – the changes would be even sharper in terms of absolute distance or of y^+ – and that it increases with distance from the wall for a given l_s^+ at a rate that varies inversely with l_s^+.

The first feature is expected since one should approach the quasi-steady regime as the imposed frequency is decreased. But, that the lag still reaches 50° at $l_s^+ = 34$ is less evident. By comparison with $\langle u \rangle$ and $\langle \tau \rangle$ whose phase shifts with respect to the imposed centreline oscillations are quite small when $l_s^+ > 20$, it is clear that the

turbulence is slower to reach the quasi-steady regime. This is somewhat similar to observations on the streamwise development of steady turbulent flows which show that the mean velocity is more rapidly established than the turbulent intensity.

The second feature, i.e. the increase of the phase lag with y^+, suggests considering the time lag

$$\Delta t^+ = (\Phi_{\widetilde{u'u'}} - \Phi_{\widetilde{uc}}) \frac{1}{\omega^+} = \tfrac{1}{2}(\Phi_{\widetilde{u'u'}} - \Phi_{\widetilde{uc}})\, l_s^{+2},$$

where the Φ are in radians. The plot of Δt^+ *vs.* y^+ of figure 14(*b*) shows that, for $y^+ > 30$, the points for the four forcing frequencies are scattered about a single straight line with a slope $\mathrm{d}y^+/\mathrm{d}(\Delta t^+) \approx 0.4$. It appears, thus, that the modulation of the turbulent intensity is propagated away from the wall with a constant speed of 0.4 wall units. This is equivalent to saying that the maximum (or the minimum) of the turbulent intensity $\langle u'u' \rangle (t/T)$ is transported away from the wall with this speed. Now, $0.5\,\mathrm{d}y^2/\mathrm{d}t$ is a diffusivity and, therefore, the diffusivity with which the maximum/minimum of $\langle u'u' \rangle$ diffuses away from the wall is

$$\nu^+_{\widetilde{u'u'}} = \frac{1}{2}\frac{\mathrm{d}y^{+2}}{\mathrm{d}t} = y^+ \frac{\mathrm{d}y^+}{\mathrm{d}t} \approx 0.4 y^+.$$

But this is exactly the value of the momentum eddy diffusivity ν_t^+ in the logarithmic layer of the mean velocity profile. Hence $\nu_{\widetilde{u'u'}} \approx \nu_t$. Furthermore, in one-point closure, like the k–ϵ model, the transport or diffusion term in the equation of the turbulent kinetic energy k is modelled as a gradient diffusion with a diffusivity $\nu_k = \nu_t/\sigma_k$, where σ_k is an empirical constant chosen such as to optimize the agreement between experimental data and predictions in some basic shear flows. The standard value of σ_k is 1, i.e. $\nu_k = \nu_t$ (Rodi 1980, pp. 28–29). Consequently, $\nu_{\widetilde{u'u'}} \approx \nu_k$, i.e. the modulation of the longitudinal turbulent energy in the inertial sublayer diffuses away from the wall with a diffusivity equal to the diffusivity of time-mean turbulent kinetic energy in the corresponding steady wall flow. Implied in this conclusion is that most of the production of $\langle u'u' \rangle$ occurs near the wall in the layer $y^+ < 30$ and that it is weak beyond. This is quite compatible with the smallness of the oscillating gradient $\langle \partial u/\partial y \rangle$ once $y^+ > l_s^+$. Also implied is that the dissipation – which accounts for the decrease of $A_{\widetilde{u'u'}}$ with y^+ – is either sufficiently small or in phase with $\langle u'u' \rangle$.

4.2.5. *Modulation of the turbulent intensity of the wall shear stress*

The data on the amplitude $A_{\widetilde{\tau'\tau'}}$ and on the phase shift $\Phi_{\widetilde{\tau'\tau'}} - \Phi_{\widetilde{uc}}$ of the modulation of the phase-averaged turbulent wall shear stress fluctuations $\langle \tau'\tau' \rangle$ is plotted *vs.* l_s^+ on figures 15(*a*) and 15(*b*). Various normalizations were tried for $A_{\widetilde{\tau'\tau'}}$. The most satisfactory one is $\bar{\tau} A_{\tilde{\tau}}$, applied in figure 15(*a*), rather than $\bar{\tau}^2$ as previously used by Binder *et al.* (1985*b*). Indeed

$$\frac{A_{\widetilde{\tau'\tau'}}}{\bar{\tau} A_{\tilde{\tau}}} = \frac{\overline{\tau'\tau'}}{\bar{\tau}^2} \frac{a_{\widetilde{\tau'\tau'}}}{a_{\tilde{\tau}}} \approx (0.35)^2 \frac{a_{\widetilde{\tau'\tau'}}}{a_{\tilde{\tau}}},$$

and $a_{\widetilde{\tau'\tau'}}/a_{\tilde{\tau}}$ may be interpreted as the response of the turbulence to the forcing $\langle \tau \rangle$. In the quasi-steady limit $\langle \tau'\tau' \rangle / \langle \tau \rangle^2$ must be independent of time. This ratio may be written as follows after expanding:

$$\frac{\langle \tau'\tau' \rangle}{\langle \tau \rangle^2} = \frac{\overline{\tau'\tau'}}{\bar{\tau}^2} \frac{1 + \widetilde{\tau'\tau'}/\overline{\tau'\tau'}}{(1 + \frac{1}{2}a_\tau^2) + 2\tilde{\tau}/\bar{\tau} + (\tilde{\tau}^2/\bar{\tau}^2 - \frac{1}{2}a_\tau^2)}.$$

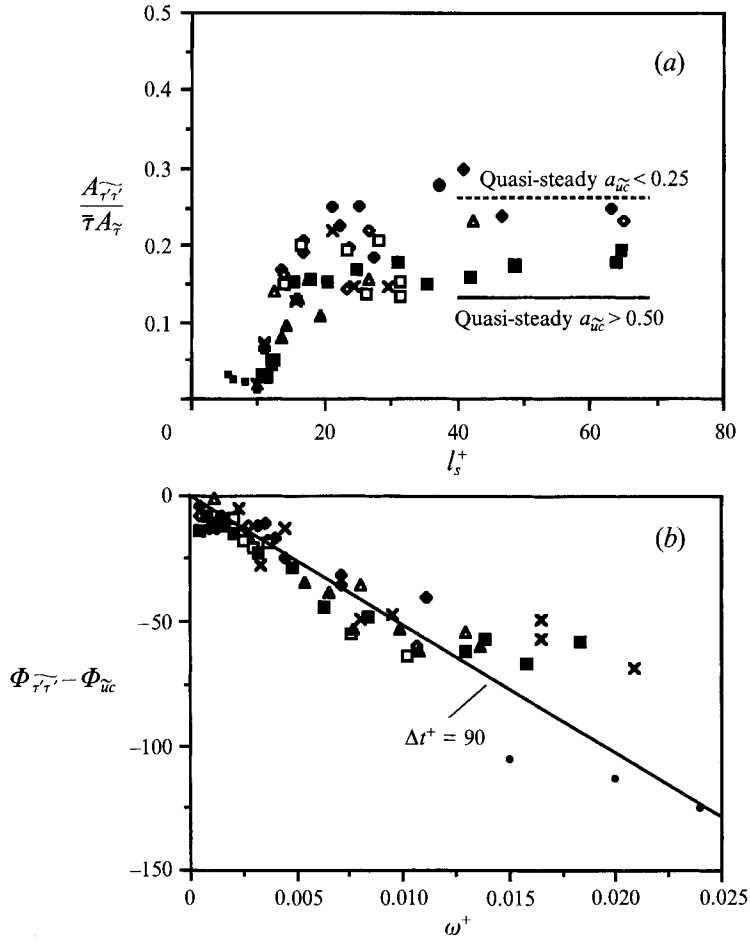

FIGURE 15. Modulation of the turbulent fluctuations of the wall shear stress. For legend see table 3. (*a*) Amplitude. (*b*) Phase shift.

Noting that $$\overline{\tilde{\tau}^2} = \tfrac{1}{2}A_{\tilde{\tau}}^2$$

if higher harmonics are neglected, the term $\frac{1}{2}a_{\tilde{\tau}}^2$ is added and subtracted in the denominator in order to make the average variation over the cycle zero. If only the first-order oscillating terms are retained, this expression becomes

$$\frac{\langle \tau'\tau' \rangle}{\langle \tau \rangle^2} = \frac{\overline{\tau'\tau'}}{\bar{\tau}^2} \frac{1}{(1+\frac{1}{2}a_{\tilde{\tau}}^2)} \frac{1+\widetilde{\tau'\tau'}/\overline{\tau'\tau'}}{1+\dfrac{2}{1+\frac{1}{2}a_{\tilde{\tau}}^2}\tilde{\tau}/\bar{\tau}}.$$

Quasi-steadiness of $\langle \tau'\tau' \rangle / \langle \tau \rangle^2$ requires than that the right-hand side is independent of time, hence

$$\frac{(\widetilde{\tau'\tau'})_{qs}}{\overline{\tau'\tau'}} = \frac{2}{1+\frac{1}{2}a_{\tilde{\tau}}^2}\frac{\tilde{\tau}}{\bar{\tau}}$$

or

$$\frac{a_{\widetilde{\tau'\tau'}qs}}{a_{\tilde{\tau}}} = \frac{2}{1+\frac{1}{2}a_{\tilde{\tau}}^2}.$$

Thus in the quasi-steady limit, i.e. $l_s^+ \to \infty$

$$\frac{(A_{\widetilde{\tau\tau}})_{qs}}{\bar{\tau}A_{\tilde{\tau}}} = (0.35)^2 \frac{2}{1+\frac{1}{2}a_{\tilde{\tau}}^2}.$$

Finally, if we substitute $a_{\tilde{\tau}(qs)} = \frac{7}{4}a_{\widetilde{uc}}$ (see §4.1), this expression becomes

$$\left(\frac{A_{\widetilde{\tau\tau}}}{\bar{\tau}A_{\tilde{\tau}}}\right)_{qs} = \frac{0.24}{1+\frac{49}{32}a_{\widetilde{uc}}^2}.$$

The values of this ratio for small amplitudes and the for the maximum centreline amplitude $a_{\widetilde{uc}} = 0.70$ are respectively 0.24 and 0.14. These values are shown on figure 15(*a*). It is seen that the experimental results follow these predicted trends. Considering the approximations required and the experimental scatter in these measurement one would not expect better qualitative agreement.

The most striking feature of figure 15(*a*) is the sharp decline of the amplitude at the lower values of l_s^+, i.e. at the higher forcing frequencies, as was observed for the turbulent velocity fluctuations discussed in the previous section. The attenuation of the modulation of the turbulent wall shear stress fluctuation is, however, sharper than that of the velocity fluctuations: there seems to be a real cutoff at $l_s^+ \approx 10$.

Analysis of the phase shift data showed that the time lag,

$$\Delta t^+_{\widetilde{\tau\tau}} = -(\Phi_{\widetilde{\tau\tau}} - \Phi_{\widetilde{uc}})/\omega^+,$$

was a constant irrespective of the frequency or of the amplitude of forcing. The plot of $\Phi_{\widetilde{\tau\tau}} - \Phi_{\widetilde{uc}}$ *vs.* ω^+ rather than l_s^+ is, therefore, more appropriate. Figure 15(*b*) indeed shows a good collapse of the data points about a single straight line. The slope of this line corresponds to $\Delta t^+ = 90$. This time is smaller than the relaxation time $T_m^+ = 200$ of the model proposed by Mao & Hanratty (1985). On the other hand, according to this model, the modulation of the turbulence should begin to decrease when $T^+ < T_m^+$, i.e. once $l_s^+ < 8$. The measurements show that the response of the turbulence in the viscous sublayer has already started to fall off at $l_s^+ = 15$ and in some instances at $l_s^+ = 20$, which correspond to forcing periods $T^+ = 700$ and $T^+ = 1200$ that are quite a bit larger than the relaxation time. This observation points into the same direction as the remark made in the previous section about the damping of $A_{\widetilde{u'u'}}$ which begins at frequencies that are larger than the energy-containing eddies.

4.2.6. *Comparison of the frequency response of the turbulent velocity and wall shear stress fluctuations*

The response of the modulation of the turbulence has been further investigated by making hot-film measurements at $y^+ = 15$ where the maximum amplitude $A_{\widetilde{u'u'}}$ occurs for nine different frequencies and for four amplitudes: $l_s^+ = 7.3$, 8, 9.5, 12, 16, 24, 30, 44, 60; $a_{\widetilde{uc}} = 0.1$; 0.2; 0.3; 0.4. At the small values of l_s^+ (7.3 and 8) the data were only gathered at the 20% amplitude because of the mediocre measurement accuracy near or in conditions of flow reversal. Simultaneous velocity and wall shear stress measurements were performed in the 20% amplitude flows.

The responses of the turbulence at $y^+ = 15$ and at $y^+ = 0$, $a_{\widetilde{u'u'}}/a_{\tilde{u}}$ and $a_{\widetilde{\tau\tau}}/a_{\tilde{\tau}}$ are plotted on figure 16(*a*). The LDV results for $a_{\widetilde{uc}} = 0.64$ discussed earlier (figure 13) are also shown on the figure. The decrease of the response with frequency is again clearly demonstrated. Noteworthy is the grouping of the values of $a_{\widetilde{u'u'}}/a_{\tilde{u}}$ *vs.* ω^+ for the different amplitudes about a single curve when $\omega^+ > 0.008$, which points to an apparently linear dependence of the turbulence on the local value of the velocity oscillation and not on the centreline velocity. There is obviously scatter of the data

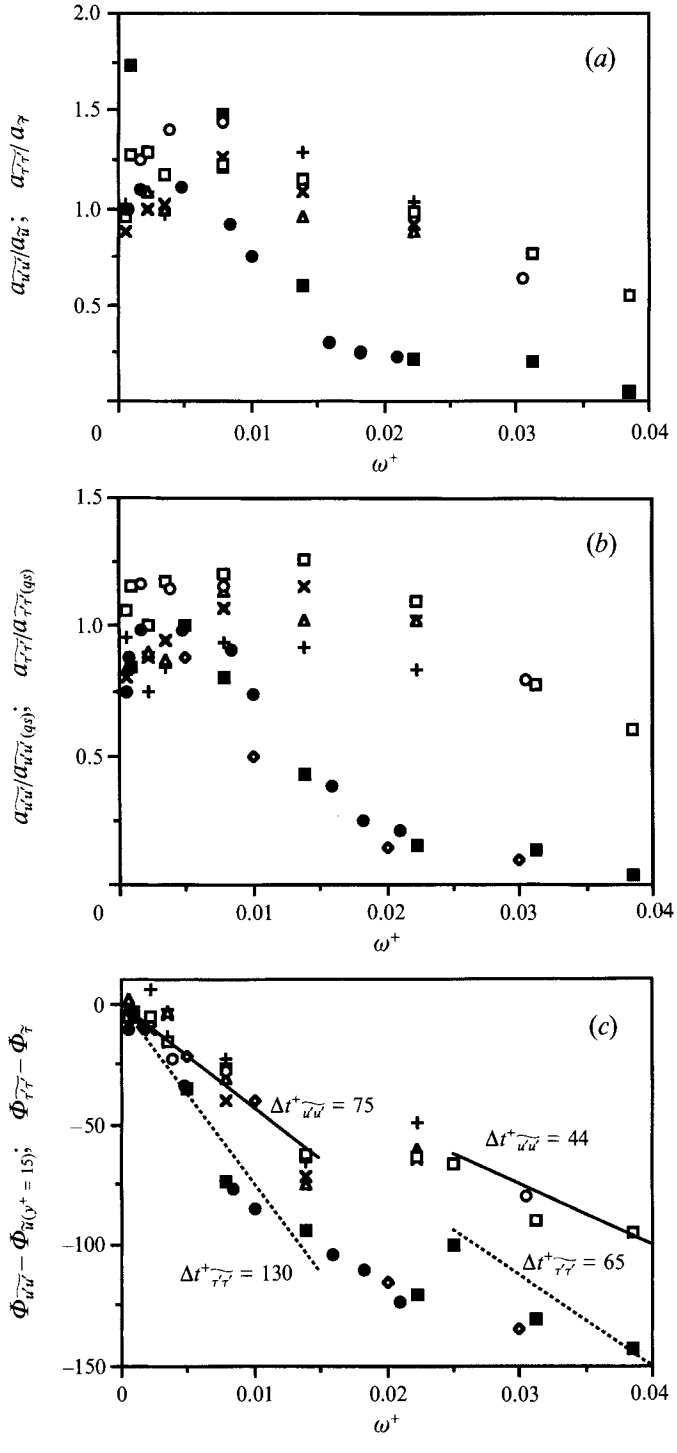

FIGURE 16. Modulation of the turbulent intensities of the velocity at $y^+ = 15$ and of the wall shear stress *vs.* forcing frequency. (*a*) Ratios of relative amplitudes. (*b*) Ratios with respect to the quasi-steady values. (*c*) Phase shifts: $a_{\widetilde{uc}} = +$, 0.10 (turb. intensity); $\times$, 0.30 (turb. intensity); $\triangle$, 0.40 (turb. intensity); $\square$, 0.20 (turb. intensity); $\bigcirc$, 0.64 (turb. intensity); $\blacksquare$, 0.20 (wall sh. stress int.); $\bullet$, 0.70 (wall sh. stress int.); $\diamond$, Finnicum & Hanratty (1988).

points about this curve but it should be judged by keeping in mind that the ratio $a_{\widetilde{u'u'}}/a_{\tilde{u}}$ involves four different quantities. The larger scatter at low forcing frequencies may indicate *a contrario* that other factors beside $a_{\tilde{u}}$ influence the modulation of turbulence.

It is seen on figure 16(*a*) that the response of the turbulent wall shear stress fluctuations differs from that of the turbulent velocity fluctuations at $y^+ = 15$, namely it begins to decline at lower forcing frequencies and decreases more rapidly with ω^+. In the quasi-steady regime and in the small-amplitude approximation one should have

$$a_{\widetilde{\tau'\tau'}} = \tfrac{7}{8}a_{\tilde{\tau}} = \tfrac{7}{4}a_{\widetilde{uc}}.$$

The value $a_{\widetilde{\tau'\tau'}}/a_{\tilde{\tau}} = 1.75$ at the lowest frequency in the $a_{\widetilde{uc}} = 0.20$ case is thus exactly equal to the quasi-steady limit.

Another representation of the same data is shown on figure 16(*b*) where the relative amplitudes of the turbulence modulation are normalized with the corresponding quasi-steady values. $a_{\widetilde{\tau'\tau'}(qs)}$ has been computed from the relationship developed in the previous section. The relative amplitude of the modulation $a_{\widetilde{u'u'}(qs)}$ at the fixed position $y^+ = 15$ is computed by assuming that the distribution $\langle u'u'\rangle/\langle u_\tau^2\rangle = f(\langle y^+\rangle)$ is independent of time – which implies zero phase shift between $\langle u'u'\rangle$ and $\langle\tau\rangle$ – and is the same as in steady flow. For convenience we write $\langle y^+\rangle = y\langle u_\tau\rangle/\nu$. Since $\langle y^+\rangle$ varies during the cycle, $\langle u'u'\rangle$ varies as the product $f(\langle y^+\rangle)\langle u_\tau^2\rangle$. Thus, if during the cycle the representative point stays on a portion of the f *vs.* y^+ curve where f is either an increasing, a constant or a decreasing function of y^+, then $a_{\widetilde{u'u'}}$ is either larger, equal to or smaller than $a_{\tilde{\tau}}$. For instance near the wall in the region $y^+ < 12$ where $(u'u')^{\frac{1}{2}}/\bar{u}_\tau \propto y^+$, one obtains if $\langle y^+\rangle < 12$ at all times

$$\langle u'u'\rangle \propto \langle u_\tau^2\rangle\langle y^{+2}\rangle \propto \langle u_\tau^4\rangle,$$

i.e. $a_{\widetilde{u'u'}(qs)} \approx 2a_{\tilde{\tau}(qs)}$. On the other hand, about the mean position $y^+ = 15$ of interest here which is on the decreasing portion of f, $a_{\widetilde{u'u'}(qs)} \approx 0.8a_{\tilde{\tau}(qs)}$. The $\overline{(u'u')^{\frac{1}{2}}}/\bar{u}_\tau$ *vs.* y^+ distribution measured by Johansson & Alfredsson (1982) was used too for the computation of $a_{\widetilde{u'u'}(qs)}$. The distribution in the range $0 < y^+ < 50$ was divided into three parts and a least-squares linear approximation was fitted to each.

The plot of figure 16(*b*) which shows trends very similar to those of figure 16(*a*) serves to emphasize the fact that the modulation of the turbulence is a monotonically decreasing function of the forcing frequency. Also shown on this figure are the measurements of Finnicum & Hanratty (1988) obtained with the electrochemical technique. The values of $A_{\widetilde{(\tau'\tau')^{\frac{1}{2}}}}/\bar{\tau}$ of these authors have been converted to $a_{\widetilde{\tau'\tau'}}/a_{\widetilde{\tau'\tau'}(qs)}$ by making the linear assumption which yields $a_{\widetilde{(\tau'\tau')^{\frac{1}{2}}}} = \frac{1}{2}a_{\widetilde{\tau'\tau'}}$ and the assumption $a_{\widetilde{\tau'\tau'}(qs)} = 4a_{\widetilde{uc}}$. It is seen that the results of these authors agree remarkably well with the present ones. The small increases in the lower frequency range in a few cases for $a_{\widetilde{uc}}$ are smaller than the experimental uncertainty and therefore not significant. The increase in the modulation of the turbulence observed by Shemer, Wygnanski & Kit (1985) is, therefore, not confirmed by the present measurements. These authors do, however, qualify their conclusion by pointing out that the absolute differences due to changes of the forcing frequency were always small. The contradiction between the two sets of observations may, hence, be more apparent than real. Finally let us point out that the characteristics of the response of the wall shear stress intensity when the imposed frequency is further increased change considerably as reported by Finnicum & Hanratty (1988) and confirmed recently by Tardu & Binder (1993).

The differences in the amplitude response of $\langle\tau'\tau'\rangle$ and $\langle u'u'\rangle$ pointed out on figure 16(*a*) are even more contrasted on figure 16(*b*). The lower-frequency response of $\langle\tau'\tau'\rangle$

with respect to that of $\langle u'u' \rangle$ implies a larger relaxation time of the turbulence in the immediate vicinity of the wall as compared to that in the buffer layer. Another manifestation of the relaxation time is the delay between the turbulence modulations and the oscillations of the corresponding quantities which at first sight may be considered as the forcing terms. The time delays inferred from the phase shift data of figure 16(*c*) are consistent with the conclusion drawn from the amplitude response, namely that the time lag of $\langle \tau'\tau' \rangle$ with respect to $\langle \tau \rangle$ is about twice as large as the lag of $\langle u'u' \rangle$ with respect to $\langle u \rangle$ at a given frequency. This figure also shows two distinct frequency regimes already alluded to in the previous section. (Note that on figure 15(*b*) the maximum frequency is only $\omega^+ = 0.02$ and that the phase shift is with respect to $\langle U_c \rangle$ and not with respect to $\langle \tau \rangle$ as on figure 16(*c*). The difference in the phase shift on the two figures corresponds therefore to the phase lead $\Phi_{\tilde{\tau}} - \Phi_{\widetilde{uc}}$.) In the high-frequency regime as $\omega^+ > 0.025$, the time lag is roughly half that in the lower one $\omega^+ < 0.015$.

It may be remarked that the end of this low-frequency regime corresponds to $l_s^+ = 12$ which is close to value $l_s^+ = 10$ where the oscillating field deviates from the Stokes solution. Even more relevant may be the observation that the beginning of the high-frequency regime is close to the average bursting frequency at $y^+ = 15$ in steady flow, $\omega_b^+ = 2\pi f_b^+ = 0.036$ (Bogard & Tiederman 1986; Coughran & Bogard 1987). It is not really unexpected that the turbulent response changes when the forcing cycle becomes shorter than the interval between the events that are responsible for a large part of the turbulence production.

The reason why the turbulence modulation in the viscous sublayer has a relaxation time that is 2 to 3 times larger than in the buffer layer is an open question. In the present work only the global response of the turbulence has been investigated. Some insight into the question would possibly be gained by analysing the spectral contents of $\langle u'u' \rangle$ and $\langle \tau'\tau' \rangle$ for different forcing frequencies. This could be done by frequency filtering the signal prior to the phase averaging. To perform such an analysis would obviously be an enormous task that is beyond the scope of this paper. As a first step, however, some characteristics of the small turbulent scales have been extracted from the $u'(t)$-signal. These results are described in the next subsection.

4.3. *Modulation of the small scales*

The Taylor microscale and the zero crossing frequency, the skewness and the flatness factors of the time derivative $\mathrm{d}u'/\mathrm{d}t$ have been determined at $y^+ = 15$ in flows forced with an amplitude $a_{\widetilde{uc}} = 20\,\%$ and at $l_s^+ = 7.2$, 9.5, 12, 16, 30 and 60.

The instantaneous turbulent fluctuation $u'(t) = u(t) - \langle u(t) \rangle$ was computed after $\langle u \rangle$ was obtained, stored on the disk of the Norsk-100 computer and processed in various ways. The time derivative was obtained with a 32-point finite-impulse-response zero-phase shift filter. The cutoff frequency of the digital derivator was set at $f^+ = 1$ in order to avoid noise contamination of the skewness and flatness factors of $\mathrm{d}u'/\mathrm{d}t$ (Kuo & Corrsin 1971).

The 'dead-band' effect on the zero-crossing frequency (due to the presence of noise which produces spurious crossings) was checked in one case by measuring the crossing frequency for four increasing levels $L\langle u'u' \rangle^{\frac{1}{2}}$. This frequency reaches a plateau near $L = 0$ showing that the S/N was adequate. The same conclusion was reached by varying the cutoff frequency of the filter.

The phase averages of the zero-crossing frequency $\langle N_0 \rangle$ of the turbulent intensity $\langle u'^2 \rangle$ and of the moments $\langle (\mathrm{d}u'/\mathrm{d}t)^n \rangle$ with $n = 2$, 3 and 4 were determined. These phase averages are statistically well converged as shown on the examples on figure 17.

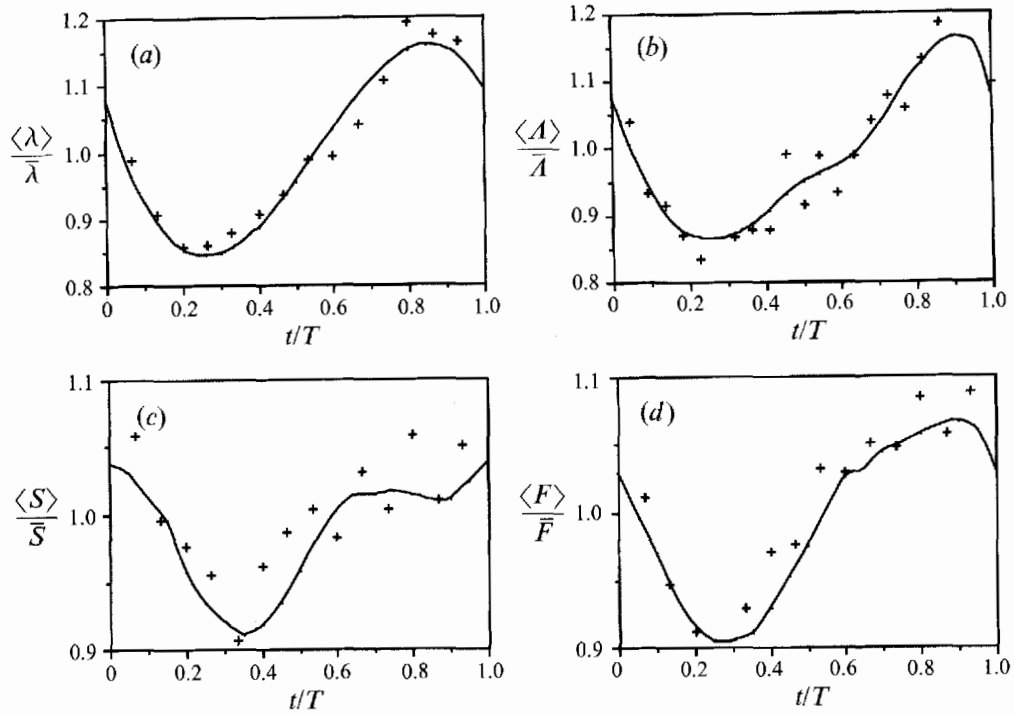

FIGURE 17. Examples of phase averages $y^+ = 15$; $a_{\widetilde{uc}} = 0.20$; $l_s^+ = 9.5$. (*a*) Taylor time microscale; (*b*) Liepmann timescale; (*c*) skewness factor of $\partial u'/\partial t$; (*d*) flatness factor of $\partial u'/\partial t$.

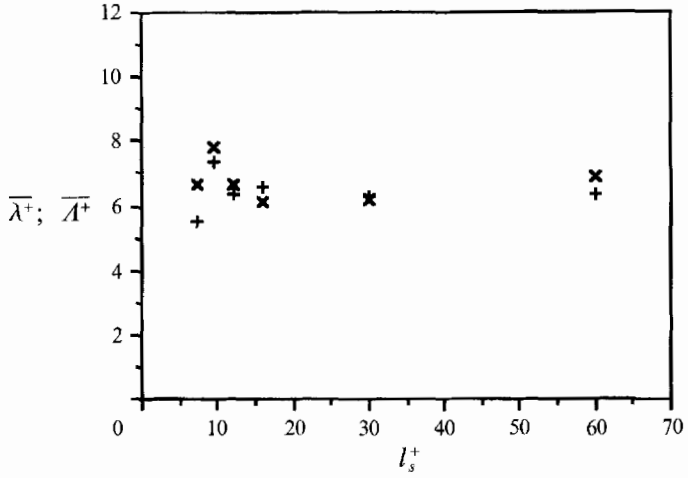

FIGURE 18. Time mean of the zero-crossing period and time-mean Taylor scale versus frequency parameter: +, $1/N_0^+$; ×, $1/2\pi\lambda^+$ ($y^+ = 15$).

For a Gaussian signal the timescale based on the zero-crossing frequency N_0: $\langle\Lambda\rangle = 1/(2\pi\langle N_0\rangle)$ is the same as the Taylor microscale

$$\lambda: \langle\lambda^2\rangle = \langle u'^2\rangle/\langle(\mathrm{d}u'/\mathrm{d}t)^2\rangle$$

(Liepmann 1949). It was experimentally established by Liepmann (1949) and Sreenivasan, Prabhu & Narasimha (1983) that the equality $\overline{\lambda^+} = \overline{\Lambda^+}$ still holds for near-

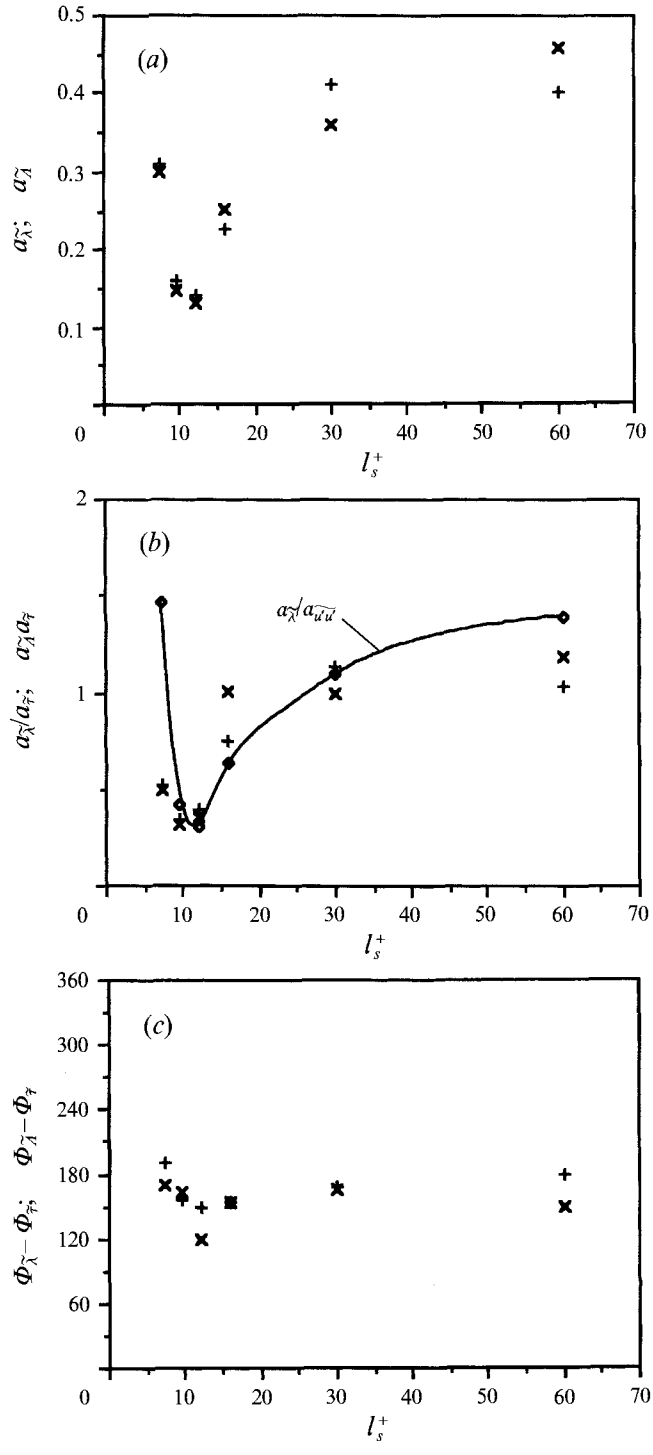

FIGURE 19. Amplitudes of the modulations of the Liepmann scales and of the Taylor microscales *vs.* frequency parameter. (*a*) Relative amplitudes. (*b*) Relative amplitudes scaled with the amplitude of the wall shear stress. (*c*) Phase shift with respect to the oscillations of the wall shear stress.

wall turbulence in steady flow despite its non-Gaussian character. Figures 18 and 19 show that this is also true in unsteady flow since the time-mean values, the amplitudes and the phase shifts of $\langle \Lambda \rangle$ and $\langle \lambda \rangle$ remain close when the forcing frequency is varied. This agreement is rather remarkable considering that the methods for determining λ and Λ are completely independent. It shows that the methods used are basically correct.

It is seen that time-mean values of the microscales $\bar{\lambda}^+$ and $\bar{\Lambda}^+$ (figure 18) are quite insensitive to the forcing over the investigated frequency range. For the cyclic variations of the microscale, it may first be remarked that in the quasi-steady regime the scaled values $\langle \lambda^+ \rangle$ should be independent of time, i.e. $\langle \lambda^+ \rangle = \bar{\lambda}^+$, if the variations due to those of the position $\langle y^+ \rangle$ may be neglected. This is only approximately the case, because as shown by Sreenivasan *et al.* (1983) $\bar{\lambda}^+$ decreases with y^+ but this decrease is by about 30% from $y^+ = 15$ until the outer edge of the logarithmic region and is almost constant in the viscous sublayer. Keeping this in mind and since the inner scaling holds in the inner layer:

$$\langle \lambda \rangle = \bar{\lambda}^+ \frac{\nu}{\langle \tau/\rho \rangle} = \bar{\lambda} \frac{1}{\langle \tau \rangle / \bar{\tau}},$$

and if the amplitudes are small

$$1 + \tilde{\lambda}/\bar{\lambda} = \frac{1}{1 + \tilde{\tau}/\bar{\tau}} \approx 1 - \tilde{\tau}/\bar{\tau}.$$

Hence in the quasi-steady small-amplitude limit one should have with inner scaling:

$$a_{\tilde{\lambda}} = a_{\tilde{\tau}}, \quad \Phi_{\tilde{\lambda}} - \Phi_{\tilde{\tau}} = 180°.$$

Figures 19(*a*) and 19(*b*) show that this is well borne out by the measurements – despite the fact $a_{\tilde{\tau}(qs)} = 2a_{\widetilde{u\tau}}$ is not very small when $l_s^+ > 30$. It is seen that the phase of $\langle \lambda \rangle$ remains nearly in opposition to the phase of $\langle \tau \rangle$ over the whole frequency range. The amplitude ratio $a_{\tilde{\lambda}}/a_{\tilde{\tau}}$, on the contrary, decreases sharply when the forcing frequency is increased with a minimum value of about 0.3 at $l_s^+ = 10$.

The micro lengthscale λ_x may be inferred from the timescale by the Taylor hypothesis $\bar{\lambda}_x^+ = \bar{u}^+ \bar{\lambda}^+$, assuming that the convection velocity of the small scales is the local mean velocity. In unsteady flow the Taylor hypothesis should be written with the phase-averaged velocity: $\mathrm{d}x = -\langle u \rangle \, \mathrm{d}t$ so that

$$\left\langle \left(\frac{\mathrm{d}u'}{\mathrm{d}x} \right)^2 \right\rangle = \left\langle \left(\frac{\mathrm{d}u'}{\langle u \rangle \, \mathrm{d}t} \right)^2 \right\rangle = \frac{1}{\langle u \rangle^2} \left\langle \left(\frac{\mathrm{d}u'}{\mathrm{d}t} \right)^2 \right\rangle$$

and hence $\langle \lambda_x \rangle = \langle u \rangle \langle \lambda \rangle$. Thus

$$\bar{\lambda}_x [1 + a_{\widetilde{\lambda x}} \cos(\omega t + \Phi_{\widetilde{\lambda x}} - \Phi_{\tilde{\tau}})] = \bar{u}\bar{\lambda}(1 + a_{\tilde{u}} \cos(\omega t + \Phi_{\tilde{u}} - \Phi_{\tilde{\tau}}))(1 + a_{\tilde{\lambda}} \cos(\omega t + \Phi_{\tilde{\lambda}} - \Phi_{\tilde{\tau}})).$$

This shows that $\bar{\lambda}^+_{x(unst)} = \bar{\lambda}^+_{x(st)}$ since both $\bar{u}^+$ and $\bar{\lambda}^+$ are not modified by forcing. Furthermore, by noticing that at $y^+ = 15$, $\Phi_{\tilde{u}} - \Phi_{\tilde{\tau}}$ is generally small, by making use of the result $\Phi_{\tilde{\lambda}} - \Phi_{\tilde{\tau}} \cong 180°$ and by assuming that the amplitudes are small, the above relation simply yields

$$a_{\widetilde{\lambda x}} \approx |a_{\tilde{\lambda}} - a_{\tilde{u}}|.$$

The amplitude of the micro lengthscale thus varies due to the combined effects of the forcing on the micro timescale and of the convection velocity. In order to find out what the relative contribution of each one is, it is best to express both in terms of the centreline amplitude in the high-frequency (HF) and low-frequency (LF) regime. For $a_{\tilde{u}}$, we have:

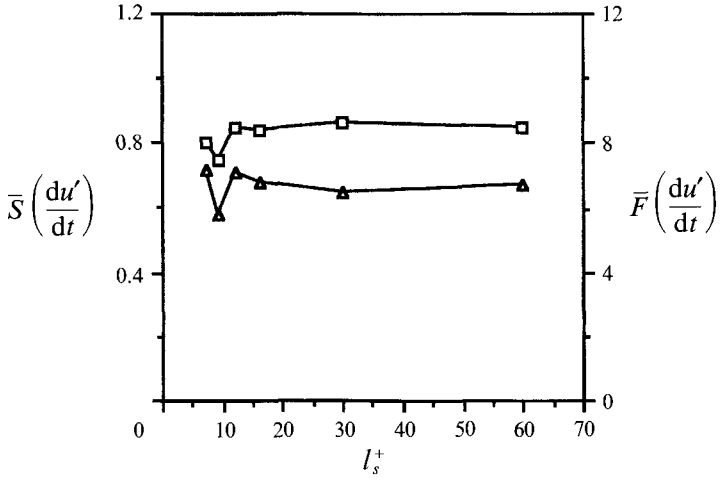

FIGURE 20. Time-mean values of skewness (□) and flatness (△) factors of $\partial u'/\partial t$ *vs.* frequency parameter.

HF $\quad a_{\tilde{u}} \approx 2a_{\widetilde{uc}}$ since at $y^+ = 15$, $A_{\tilde{u}} = A_{\widetilde{uc}}$ and $\bar{u} \approx \frac{1}{2}\bar{U}_c$;

LF $\quad a_{\tilde{u}} \approx a_{\widetilde{uc}}$ since at $y^+ = 15$, $\langle u \rangle = \langle u_\tau \rangle f(\langle y^+ \rangle) \approx \langle u_\tau \rangle$

because $\quad f(\langle y^+ \rangle) \approx f(y^+)\left(1 + \dfrac{f'(15)}{f(15)}\dfrac{\widetilde{u_\tau} y}{\nu}\right), \quad \dfrac{f'(15)}{f(15)} = \dfrac{0.6}{11} \ll 1.$

For $a_{\tilde{\lambda}}$, we deduct the value from the ratio $a_{\tilde{\lambda}}/a_{\tilde{\tau}}$ of figure 19(*b*), so we need the relation between $a_{\tilde{\tau}}$ and $a_{\widetilde{uc}}$. At

HF $\quad a_{\tilde{\tau}} = \sqrt{2}\dfrac{\bar{U}_c}{\bar{u}_\tau}\dfrac{a_{\widetilde{uc}}}{l_s^+} = 31\dfrac{a_{\widetilde{uc}}}{l_s^+}$ (see §4.2.3),

LF $\quad a_{\tilde{\tau}} \approx \frac{7}{4}a_{\widetilde{uc}}$.

Combining these results yields

at HF ($l_s^+ < 10$) $\quad a_{\widetilde{\lambda x}} = \left|\dfrac{31}{l_s^+}\dfrac{a_{\tilde{\lambda}}}{a_{\tilde{\tau}}} - 2\right| a_{\widetilde{uc}}$;

at LF ($l_s^+ > 30$) where $a_{\tilde{\lambda}} = a_{\tilde{\tau}}$ $\quad a_{\widetilde{\lambda x}} = \frac{3}{4}a_{\widetilde{uc}}$.

Thus at LF the contribution of $a_{\tilde{\lambda}}$ to $a_{\widetilde{\lambda x}}$ is nearly twice that $a_{\tilde{u}}$. On the other hand at HF the factor $31a_{\tilde{\lambda}}/a_{\tilde{\tau}}l_s^+$ which is the contribution of $a_{\tilde{\lambda}}$ is minimum when $a_{\tilde{\lambda}}/a_{\tilde{\tau}}$ is minimum since this ratio increases rapidly when l_s^+ exceeds 10 as shown by figure 19(*b*). From the measured values of this figure, it follows that $(31a_{\tilde{\lambda}}/l_s^+ a_{\tilde{\tau}})_{l_s^+=10} \approx 1$. Thus $(a_{\tilde{\lambda}}/a_{\tilde{u}})_{min} = \frac{1}{2}$, which means that at $l_s^+ = 10$ the modulation of $\langle \lambda_x \rangle$ is mainly due to the convection velocity and $a_{\widetilde{\lambda x}} = a_{\widetilde{uc}}$. The conclusion is that $\langle \lambda_x \rangle$ is mostly modulated with an amplitude which is of the same order as that of the centreline velocity. The forcing is, therefore, felt in the small scales of the turbulence. In short, the modulation of the microscale $\langle \lambda_x \rangle$ comes mainly from the convection velocity at HF and mainly from the microscale $\langle \lambda \rangle$ at LF. In the range $10 < l_s^+ < 30$, there should hence be a

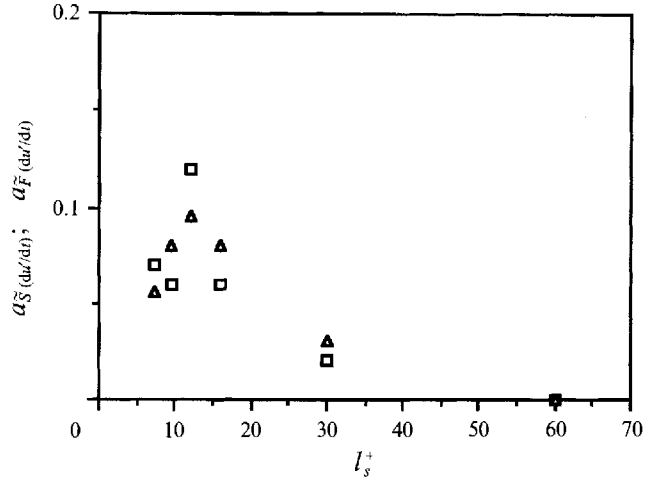

FIGURE 21. Relative amplitudes of the modulations of the skewness (□) and flatness (△) factors of $\partial u'/\partial t$.

frequency when the two contributions to $a_{\widetilde{\lambda x}}$ balance and for which $\widetilde{\lambda}_x$ should be zero or at least small. One may further remark that when $l_s^+ < 10$, $a_{\tilde{\lambda}}/a_{\tilde{u}}$ will increase again with decreasing l_s^+; actually at $l_s^+ = 7$, $a_{\tilde{\lambda}}/a_{\tilde{u}} = 1.1$, so the $a_{\widetilde{\lambda x}}$ is zero again close to $l_s^+ = 7$. Thus $a_{\widetilde{\lambda x}}$ varies rapidly in the range $l_s^+ = 7$–30.

Another aspect of the small turbulence scale is represented by the skewness S of $\mathrm{d}u'/\mathrm{d}t$ because it is directly related to the vorticity/dissipation production which is composed of terms like $(\partial u'/\partial x)^3$. It is indeed easily seen that $\langle S\rangle\,(\partial u'/\partial t) = -\langle S\rangle\,(\partial u'/\partial x)$ because of the normalization with the variance so that the convection velocity does not intervene. The mean value of $\langle S\rangle$ is about 0.85 (figure 20) and compares well with the data of Ueda & Hinze (1975) taken in steady flow. As for other quantities, the time-mean skewness is not affected by the forcing.

In discussing the modulation of $\langle S\rangle$ let us first remark that this is a structure parameter independent of any scaling and that it is independent of the Reynolds number provided this number is large enough (Kuo & Corrsin 1971). Since at low frequency the forcing affects the phase averages only via the changes of the centreline velocity and the changes of the Reynolds number, and since the profile of $\bar{S}$ is flat around $y^+ = 15$ in quasi-steady flow (Ueda & Hinze 1975), it may be expected that $\langle S\rangle$ is not modulated in this case. This is well borne out by the measurements, since the amplitude $a_{\tilde{S}}$ is effectively zero when $l_s^+ = 60$ as shown on figure 21. The constancy of $\langle S\rangle$ during the cycle implies that $\langle(\partial u'/\partial t)^3\rangle$ varies exactly in the same way as $(\langle\partial u'/\partial t)^2\rangle)^{\frac{3}{2}}$, which is effectively modulated at low frequency as was seen above in the discussion of the microscale. At high frequencies $a_{\tilde{S}}$ reaches values of the order of 10 %, i.e. $0.5a_{\widetilde{uc}}$. This may appear to be a small modulation at first sight but in view of the preceding discussion it is quite significant since it reveals a change in the internal structure of the small-scale turbulence. The amplitude $a_{\tilde{S}}$ seems to pass through a maximum at $l_s^+ = 12$. With due caution on account of the small number of data points, of the small relative variations of $\langle S\rangle$ and of the experimental uncertainty, the same critical value of the frequency parameter is found again.

The flatness factor of $\partial u/\partial t$ is related to a sort of intermittency of the turbulence. It may be seen on figure 20 that the time-average value is about 6.6 and again compares well with the steady flow data at $y^+ = 15$ of Ueda & Hinze (1975). The modulation

amplitude of $\langle F \rangle$ (figure 21) varies in the same manner with the forcing frequency as that of $\langle S \rangle$. The remarks made above concerning the low- and high-frequency behaviour of $\langle S \rangle$ are also relevant for the flatness factor.

5. Conclusion

The data on unsteady turbulent channel flow discussed in this paper have been acquired by making use of several experimental techniques and cover a significant range of forcing amplitudes and frequencies. They confirm that all the time-mean characteristics – with the sole exception of the turbulent intensity in the inertial sublayer – are not or are only slightly affected by the forcing even when the amplitude and the frequency are high enough to produce periodic flow reversal near the wall. The similarity of the oscillating velocity field $\tilde{u}$ and of the oscillating wall shear stress $\tilde{\tau}$ when the non-dimensional Stokes length l_s^+ (or equivalently the forcing frequency ω^+ expressed in wall units) is constant is also confirmed. It is shown that these periodic oscillations are affected by the turbulence only when $l_s^+ > 10$.

The turbulence itself is modulated by the forcing as is evident from the phase averages $\langle u'u' \rangle$ and $\langle \tau'\tau' \rangle$. The variations of the turbulence modulation across the flow show that it diffuses away from the wall with a diffusivity that is very close to the eddy diffusivity in the inertial sublayer. This suggests that a large part of the $\langle u'u' \rangle$-modulation is produced in the buffer layer where most of the mean turbulence energy is also produced. The frequency response of $\langle u'u' \rangle$ at $y^+ = 15$ and of $\langle \tau'\tau' \rangle$ decays when the forcing frequency increases once $l_s^+ < 20$. Moreover $\langle \tau'\tau' \rangle$ decays sooner and faster than $\langle u'u' \rangle$, showing that the relaxation time of the turbulence that filters to the wall is about two to three times larger than that in the buffer layer. Similar conclusions are reached from the time lags between the modulation of the random turbulent fluctuations and the oscillations of the corresponding deterministic quantities. These time lags are 75 and 130 wall units respectively for $\langle u'u' \rangle$ and $\langle \tau'\tau' \rangle$ when $\omega^+ < 0.012$, i.e. $l_s^+ > 13$. They decrease by nearly a factor 2 once $\omega^+ > 0.025$. It may be noted that this value approaches the bursting frequency of the mean flow $\omega_b^+ = 0.036$.

The forcing propagates to the small scales of the turbulence as is evident from the cyclic variations of the Taylor microscale and from the skewness factor of $\partial u'/\partial t$.

The evolution of several parameters reveals that critical changes in the turbulence occur in the range $l_s^+ = 10$ to 13, i.e. $\omega^+ = 0.012$ to 0.02. As was pointed out, this upper frequency approaches the mean bursting frequency. It may also be speculated that there is an optimal interaction of the oscillating flow with the turbulence in the buffer region in this frequency range since at higher frequencies this region oscillates as a plug flow with zero or small oscillating shear and at lower frequencies the quasi-steady regime is approached.

Simple quasi-steady analysis combined with the linearity assumption predicts much low-frequency behaviour remarkably well and gives at least the right trend when the forcing amplitudes are large. It shows saturation effects, as on the modulation of $\langle \tau'\tau' \rangle$ whose amplitude in the linear quasi-steady limit is four times the centreline amplitude. The quasi-steady regime is reached as soon as l_s^+ exceeds 30.

It must be emphasized that the present results concern unsteady channel flow while in most practical situations one has to deal with boundary layers and furthermore with boundary layers in pressure gradients. From the agreement of some unsteady boundary-layer results with the present data and from the fairly universal character of the turbulent flow near the wall – not withstanding some recent observations to the contrary – one may expect unsteady turbulent boundary layers to behave much as

channel flows in the inner layer. This clearly does not preclude the existence of substantial differences in the unsteady behaviour of the outer flows due to the loss of the streamwise homogeneity, and the intermittency in the wake region where the presence of the wall is felt only weakly.

This work was supported in part by the European Office of the US Army Research Development and Standardization Group (contract DAJA 45-87-C-001) and monitored by Dr R. E. Reichenbach. During part of this work R. F. Blackwelder was on leave from USC and supported as Professor Associé by the Institut National Ploytechnique de Grenoble. This support is gratefully acknowledged.

Appendix A. Wall deflections

If the periodic pressure variations $\tilde{p}$ which drive the oscillating flow produce wall deflections $\tilde{d}$ a probe which does not move with the wall will see a parasitic velocity oscillation $\widetilde{u_d}$ due to its displacement across the mean velocity profile. Since the maximum velocity gradient is $\bar{u}_\tau^2/\nu$ in the viscous sublayer:

$$\tilde{u}_d \leqslant (\bar{u}_\tau^2/\nu)\,\tilde{d}$$

and

$$A_{\tilde{u}\tilde{d}} \leqslant (\bar{u}_\tau^2/\nu)\,A_{\tilde{d}},$$

so that

$$\frac{A_{\tilde{u}\tilde{d}}}{A_{\tilde{u}}} < \frac{\bar{u}_\tau^2}{\nu}\frac{A_{\tilde{d}}}{A_{\tilde{u}}} = \frac{A_{\tilde{d}}^+}{A_{\tilde{u}}^+},$$

where $(\,)^+$ designates a quantity scaled with inner variables as usual. Hence, the relative error on the measured velocity amplitude is of order of $A_{\tilde{d}}^+/A_{\tilde{u}}^+$. Under given forcing conditions the error is proportionally worse as the wall is approached since $A_{\tilde{u}}^+$ tends to zero and it is likely to be more severe when the viscous lengthscale $\nu/\bar{u}_\tau$ is smaller. It is possible that such wall deflections were sufficiently important in the experiment of Acharya (1975) to account for the surprising shape of the $A_{\tilde{u}}$ and $\Phi_{\tilde{u}}$ profiles of this author in the high-frequency case.

In order to check the magnitude of the periodic displacement of the wall, measurements were made with an ultrasonic depth gauge having a sensitivity of 1 μm (figure 22). If the imposed frequency is small compared to the resonance frequency of the structure, as is the case here, the amplitude of the displacement should be proportional to the driving force $\tilde{p}$ and, therefore, to $\omega A_{\widetilde{uc}}$. It is seen from figure 22 that indeed $A_{\tilde{d}}(\mu\text{m}) = 2f(\text{Hz})\,A_{\widetilde{uc}}(\text{cm s}^{-1})$. This gives a maximum error of less than 10% in the most unfavourable case corresponding to $f = 0.4$ Hz.

Appendix B. Correction of the statistical bias effect in the LDA measurements

The correction of the statistical bias in velocity measurements performed with LDA is performed in a simplified manner by simultaneously determining the time-mean Doppler frequency and the average Doppler period. Consider a population of measured velocities over which averages are determined. On the histogram of this population, let n_i be the number of samples of the class u_i. If the concentration of scattering particles is homogeneous,the number of measurement is proportional to the

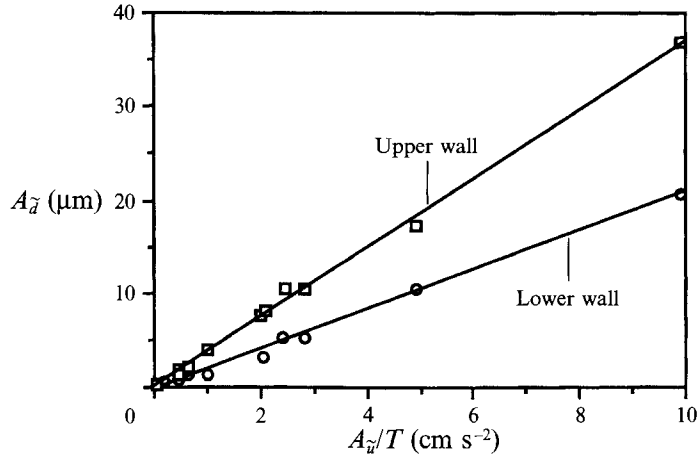

FIGURE 22. Amplitude of the periodic wall deflections produced by the oscillating pressure.

flux of particles through the probe volume, i.e. $n_i = ku_i$. Then the measured (index m) moment of order p is

$$(\overline{u^p})_m = \frac{\sum\limits_i n_i u_i^p}{\sum\limits_i n_i} = \frac{\sum\limits_i u_i^{p+1}}{\sum\limits_i u_i} = \frac{\overline{u^{p+1}}}{\bar{u}},$$

where u^{p+1} is the true moment of order $p+1$. Let d_f be the fringe spacing, f_D and t_D be the measured Doppler frequency and period, so that $u_i = d_f f_{Di} = d_f/t_{Di}$. For $p = 1$, by substituting $u = u + u'$ in the above formula, one obtains

$$(\bar{u})_m = d_f(\overline{f_D})_m = \frac{\overline{u^2}}{\bar{u}} = \bar{u}\left(1 + \frac{\overline{u'^2}}{\bar{u}^2}\right).$$

Thus the average Doppler frequency yields a biased value of the mean velocity as shown by McLaughlin & Tiederman. For $p = -1$, however,

$$\overline{\left(\frac{1}{u_m}\right)} = \frac{\overline{(t_D)_m}}{d_f} = \frac{1}{\bar{u}} \quad \text{or} \quad \bar{u} = \frac{d_f}{\overline{(t_D)_m}},$$

which shows that the true unbiased mean velocity may simply be obtained from the average Doppler period. This is especially interesting because counters actually determine the Doppler period.

The mean velocity and turbulent intensity were, thus, computed from the average Doppler period and frequency according to the two relations:

$$\bar{u} = \frac{d_f}{\overline{(t_D)_m}}, \qquad \overline{u^2} = \bar{u}^2 + \overline{u'^2} = d_f^2 \frac{\overline{(f_D)_m}}{\overline{(t_D)_m}}.$$

Similar relations apply to the ensemble or phase averages.

Appendix C. Response of the thermal boundary layer over the hot film with flow reversal

The effect of the heat transfer into the substrate was negligible in the present working conditions. The attenuation of the frequency response in the most unfavourable case corresponding to $\omega^* = 0.5$ was only 4% (with $Pe = 18$) as given by the computations

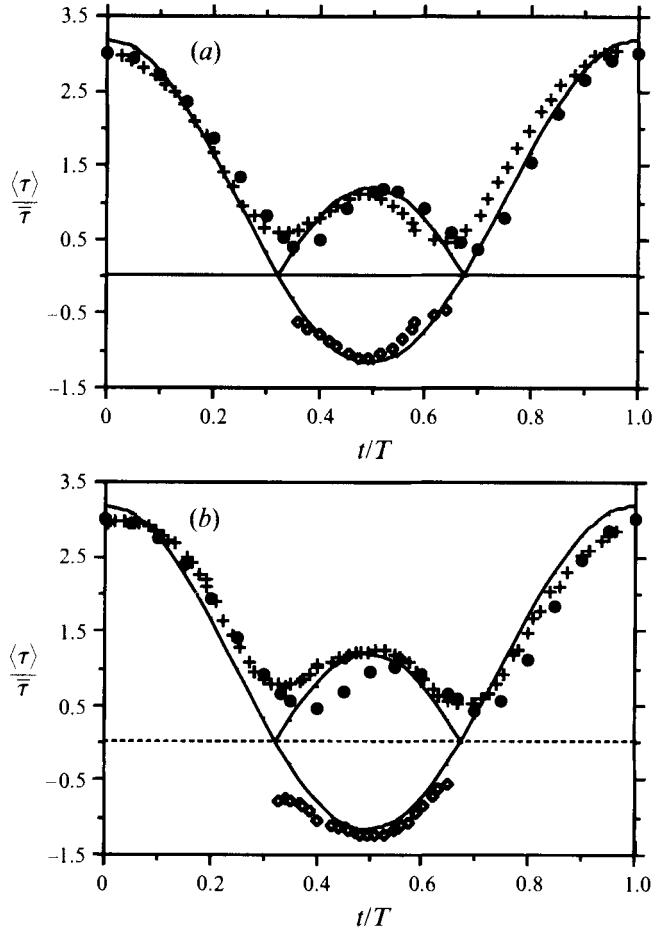

FIGURE 23. Comparison of the measurements of the modulation of the wall shear stress with the computations of Tardu *et al.* (1985). $Pe = 12$, $a_{\tau} \approx 2$. (*a*) $l_s^+ = 7$, (*b*) $l_s^+ = 5$. +, Measurements; ●, computations; ◇, rectification.

of the full heat transfer problem in the fluid and the solid carried out by Tardu, Pham & Binder (1991) in the case of a glass(substrate)/water(fluid) combination.

The axial diffusion could, however, not be ignored since the time-mean Péclet number is small. In such a case the Levêque $\frac{1}{3}$ law has to be corrected by

$$Nu \propto Nu_{Lev} + O(Pe^{-\frac{1}{6}}) \propto Pe^{\frac{1}{3}} + O(Pe^{-\frac{1}{6}})$$

i.e. the effect of the axial diffusion varies like $Pe^{-\frac{1}{6}}$. Ling (1963) has, for instance, proposed the following relationship:

$$Nu = 0.807\, Pe^{\frac{1}{3}} + 0.19\, Pe^{-\frac{1}{6}}$$

when Pe is small. In the quasi-steady limit and with $a_{\widetilde{uc}} = 0.64$ the minimum Pe during the oscillation cycle is about 2.5 in these measurements. The difference between the Levêque solution and the computations and measurements of Ackerberg, Patel & Gupta (1978) for this Pe value is less than 14%. This slight difference combined with the fact that the axial diffusion is somewhat taken into account in the *in situ* calibrations with $E^2 = A + B\overline{\tau}^n$ shows that the error in the measurements of $\langle\tau\rangle$ in the low-imposed-frequency range is less than 10%.

In the high-imposed-frequency regime wherein flow reversal occurs the situation is more complicated. Let us recall that the axial diffusion, which may become important near flow reversal, in particular when the time-mean *Pe* number is small, is not taken into account in the previous computations of Kaiping (1983). If $\overline{Pe}$ is large it is likely that the effects of the thermal wake and the thermal inertia dominate the axial diffusion near the reversal points but this has to be confirmed. On the other hand, the effect of the thermal wake over the hot film during the flow reversal and the axial diffusion are both omitted in the theoretical work of Pedley (1976). That is the reason why a complete numerical solution of the problem was undertaken by Tardu, Binder & Blackwelder (1985) and these results will be published elsewhere (Pham 1992). Let us make a few comments here with a typical example. Figure 23 compares the measurements with the computations for $Pe = 12$, $a_{\tilde{\tau}} \approx 2$ respectively for $\omega^* = 2Pe^{\frac{1}{3}}/l_s^{+2} = 0.1$ ($l_s^+ = 7$) and $\omega^* = 0.2$ ($l_s^+ = 5$). These conditions are much more severe than those investigated in this study. For $l_s^+ = 7$ the solution of the full equation agrees well with the experimental results (figure 23*a*). This is somewhat surprising because high turbulent fluctuations are present in the experiments, but the computation is fully laminar. At the highest imposed frequency, there is a phase lag near the first reversal point (figure 23*b*). In both cases the behaviour of $\langle\tau\rangle$ is surprisingly close to the quasi-steady behaviour (taking account of the axial diffusion) in the reversal phase except near the reversal points. The imposed frequency at which true unsteady effects appear in the response of the thermal boundary layer is much higher than the maximum investigated here ($l_s^+ < 3$; Tardu *et al.* 1985; Pham 1992). This justifies the rectification of $\langle\tau\rangle$ with respect to zero as shown in figure 23(*b*). This procedure has caused negligible harmonic distortion in the phase average of the wall shear stress modulation in the present working conditions.

REFERENCES

ACHARYA, M. 1975 Measurements and predictions of a fully developed turbulent channel flow with imposed controlled oscillations. PhD Thesis, Stanford University, Dept. Mech. Engineering.

ACKERBERG, R. C., PATEL, R. D. & GUPTA, S. K. 1978 The heat/mass transfer to a finite strip at small Péclet numbers. *J. Fluid Mech.* **86**, 49.

BINDER, G. & KUENY, J. L. 1981 Measurements of the periodic velocity oscillations near the wall in unsteady turbulent channel flow. In *Unsteady Turbulent Shear Flows* (ed. R. Michel, J. Cousteix & R. Houdeville), p. 100. Springer.

BINDER, G., TARDU, S., BLACKWELDER, R. F. & KUENY, J. L. 1985*a* Etude expérimentale de couches limites turbulentes instationnaires soumises à des gradients de pression moyens nuls ou positifs. *Agard Symposium on Unsteady Aerodynamics Fundamentals and Applications to Aircraft Dynamics; Conf. Proc.* 386.

BINDER, G., TARDU, S., BLACKWELDER, R. F. & KUENY, J. L. 1985*b* Large amplitude periodic oscillations in the wall region of a turbulent channel flow. *Proc. Fifth Symposium on Turbulent Shear Flows.* Cornell University.

BLACKWELDER, R. F. & HARITONIDIS, J. H. 1983 Scaling of the bursting frequency in turbulent boundary layers. *J. Fluid Mech.* **132**, 87.

BOGARD, D. G. & TIEDERMAN, W. G. 1986 Burst detection with single point velocity measurements. *J. Fluid Mech.* **162**, 389.

BRERETON, G. J. & REYNOLDS, W. C. 1987 Experimental study of the fluid mechanics of unsteady turbulent boundary layers. *Rep.* TF-29. Thermosciences Division, Department of Mechanical Engineering, Stanford University, Stanford.

BRERETON, G. J. & REYNOLDS, W. C. 1991 Dynamic response of boundary-layer turbulence to oscillatory shear. *Phys. Fluids* **3**, 178.

BRERETON, G. J. & REYNOLDS, W. C. & JARAYAMAN, R. 1990 Response of a turbulent boundary layer to sinusoidal free-stream unsteadiness. *J. Fluid Mech.* **221**, 131.

CARR, W. 1981 A review of unsteady turbulent boundary-layer experiments. *NASA Tech. Mem.* 81297. Also in *Unsteady Turbulent Shear Flows* (ed. R. Michel, J. Cousteix & R. Houdeville), p. 3. Springer.

CHAMBERS, F. W., MURPHY, H. D. & MCELIGOT, D. M. 1983 Laterally converging flow. Part 2. Temporal wall shear stress. *J. Fluid Mech.* **127**, 403.

COLES, D. 1978 A model for flow in the viscous sublayer. In *Coherent Structures of Turbulent Boundary Layers. AFOSR/Lehigh University Workshop* (ed. C. R. Smith & D. E. Abbott), pp. 462–475. Dept. Mechanical Engineering and Mechanics, Lehigh Un., Bethlehem.

COMPTE-BELLOT, G. 1965 *Ecoulement Turbulent entre deux Parois Parallèles.* Publications Scientifiques et Techniques de l'Air.

COUGHRAN, M. T. & BOGARD, D. G. 1987 An experimental study of the burst structure in a LEBU-modified boundary-layer. *10th Symp. on Turbulence, Rolla, Missouri, September 1987*, p. 45–1.

COUSTEIX, J. & HOUDEVILLE, R. 1985 Turbulence and skin friction evolutions in an oscillating boundary layer. *Proc. Fifth Symp. on Turbulent Shear Flows, Cornell University, USA.*

COUSTEIX, J., HOUDEVILLE, R. & JAVELLE, J. 1977 Structure and development of a turbulent boundary layer in an oscillatory external flow. *Proc. First Symp. on Turbulent Shear Flows, Pennsylvania State University.*

COUSTEIX, J., JAVELLE, J. & HOUDEVILLE, R. 1981 Influence of Strouhal number on the structure of flat plate turbulent boundary layer. *Proc. Third Symp. on Turbulent Shear Flows, University of California, Davis.*

ECKELMANN, H. 1974 The structure of the viscous sublayer and the adjacent wall region in a turbulent channel flow. *J. Fluid Mech.* **132**, 87.

FINNICUM, D. S. & HANRATTY, T. J. 1988 Effect of imposed sinusoidal oscillations on turbulent flow in a pipe. *PhysicoChem. Hydrodyn.* **10** (5/6), 585.

HOUDEVILLE, R., JULLIEN, J. E. & COUSTEIX, J. 1984 Mesure du frottement pariétal par jauges à elements chauds. *La Recherche Aérospatiale*, 1984–1.

JAYARAMAN, R., PARIKH, P. & REYNOLDS, W. C. 1982 An experimental study of the dynamics of an unsteady turbulent boundary layer. *Rep.* TF-18. Dept. Mech. Engng, Stanford University.

JOHANSSON, A. V. & ALFREDSSON, P. H. 1982 On the structure of turbulent channel flow. *J. Fluid Mech.* **122**, 295.

KAIPING, P. 1983 Unsteady forced convective heat transfer from a hot film in non-reversing and reversing shear flow. *Intl J. Heat Mass Transfer* **26**, 545.

KARLSSON, K. F. 1959 An unsteady turbulent boundary layer. *J. Fluid Mech.* **5**, 622.

KIM, J., MOIN, P. & MOSER, R. 1987 Turbulence statistics in fully developed channel flow at low Reynolds number. *J. Fluid Mech.* **177**, 133–166.

KUO, A. Y. S. & CORRSIN, S. 1971 Experiments on internal intermittency and fine-structure distribution functions in fully turbulent flow. *J. Fluid Mech.* **50**, 285.

LIEPMANN, H. W. 1949 Die Anwendung eines Satzes über die Nullstellen Stochastishcer Funktionen auf Turbulenzmessungen. *Helv. Phys. Acta* **22**, 119.

LING, S. C. 1963 Heat transfer from a small isothermal spanwise strip on an insulated boundary. *Trans. ASME* C: *J. Heat Transfer* **85**, 230.

LOUIS, B. & ISABEY, D. 1990 Impedance of laminar oscillatory flow superimposed on a continuous turbulent flow. In *Application to Respiratory Impedance Measurements in Respiratory Biomechanics* (ed. M. A. F. Epstein & J. R. Ligas), pp. 57. Springer.

MAO, Z.-X. & HANRATTY, T. J. 1986 Studies of the wall shear stress in a turbulent pulsating pipe flow. *J. Fluid Mech.* **170**, 545.

MAO, Z.-X. & HANRATTY, T. J. 1991 Measurement of wall shear rate in large amplitude unsteady reversing flows. In *Proc. Eight Symp. on Turbulent Shear Flows, Munich, Sept. 9–11, 1991*, pp. 11-1-1; 11-1-3.

MCLAUGHLIN, D. K. & TIEDERMAN, W. G. 1973 Biasing correcting for individual realization of laser anemometer measurements in turbulent flows. *Phys. Fluids* **16**, 2082.

MENENDEZ, A. N. & RAMAPRIAN, B. R. 1983 Study of unsteady turbulent boundary layers. *IIHR Rep.* 270. The University of Iowa.

MIZUSHINA, T., MARUYAMA, T. & HIPSAWA, H. 1975 Structure of the turbulence in pulsating pipe flows. *J. Chem. Engng Japan* **8**, 210.

MIZUSHINA, T., MARUYAMA, T. & SHIOZAKI, Y. 1973 Pulsating turbulent flow in a tube. *J. Chem. Engng Japan* **6**, 487.

PARIKH, P. G., REYNOLDS, W. C., JAYARAMAN, R. & CARR, L. W. 1981 Dynamic behaviour of an unsteady turbulent boundary layer. *Proc. IUTAM Symp. on Unsteady Turbulent Shear Flows, Toulouse May 5–8, 1981.*

PEDLEY, T. J. 1976 Transfer from a hot film in reversing shear flow. *J. Fluid Mech.* **78**, 513.

PHAM, C. T. 1992 Simulation numérique de la réponse du film chaud pariétal. PhD thesis, University of Grenoble.

RAMAPRIAN, B. R. & TU, S. W. 1983 Fully developed periodic turbulent pipe flow. *J. Fluid Mech.* **137**, 59.

RODI, W. 1980 *Turbulence Models and their Application in Hydraulics – A State of the Art Review.* Intl Association of Hydraulic Research Monograph, Delft.

RONNEBERGER, D. & AHRENS, C. D. 1977 Wall shear stress caused by signal amplitude perturbations of turbulent boundary-layer flow: an experimental investigation. *J. Fluid Mech.* **83**, 433.

SANDBORN, V. A. 1979 Evaluation of the time dependent surface shear stress in turbulent flows. *Paper* 79-WA/FE-17, *ASME Winter Annual Meeting, New York.*

SHEMER, L., WYGNASKI, E. K. & KIT, E. 1985 Pulsating flow in a pipe. *J. Fluid Mech.* **153**, 313.

SPALART, P. R. 1988 Direct simulation of a turbulent boundary layer up to $Re_\theta = 1410$. *J. Fluid Mech.* **187**, 61.

SPENCE, D. A. & BROWN, G. L. 1968 Heat transfer to a quadratic shear profile. *J. Fluid Mech.* **33**, 753.

SREENIVASAN, K. R., PRABHU, A. & NARASIMHA, R. 1983 Zero-crossings in turbulent signals. *J. Fluid Mech.* **137**, 251.

TARDU, S. 1988 Ecoulement turbulent instationnaire près d'une paroi; réponse des structures turbulentes. PhD thesis, University Joseph Fourier, Grenoble I.

TARDU, S. & BINDER, G. 1993 Wall shear stress modulation in unsteady turbulent channel flow with high imposed frequencies. *Phys. Fluids* A **5**, 2028.

TARDU, S., BINDER, G. & BLACKWELDER, R. F. 1985 Wall shear stress measurements in reversing oscillatory turbulent boundary layers. *Euromech 202 Conference on Measurement Techniques in Low-Speed Flows; 7–10 October 1985, N.L.R. Netherlands.*

TARDU, S., BINDER, G. & BLACKWELDER, R. F. 1986 An experimental investigation of LDA bias using a large amplitude oscillatory channel flow. *Third Intl Symp. on Applications of Laser Anemometry to Fluid Mechanics, Lisbon, Portugal.*

TARDU, S., BINDER, G. & BLACKWELDER, R. F. 1987 Modulation of bursting by periodic oscillations imposed on channel flow. *Proc. Sixth Symp. on Turbulent Shear Flows, Université Paul Sabatier, Toulouse, France*, p. 4.5.1.

TARDU, S., PHAM, C. T. & BINDER, G. 1991 Effects of longitudinal diffusion in the fluid and of heat conduction to the substrate on the response of wall hot-film gauges. In *Advances in Turbulence 3* (ed. A. V. Johansson & P. H. Alfredsson), pp. 506–513. Springer.

TU, S. W. & RAMAPRIAN, B. R. 1983 Fully developed periodic turbulent pipe flow. Part 1. Main experimental results and comparison with predictions. *J. Fluid Mech.* **137**, 31.

UEDA, H. & HINZE, J. O. 1975 Fine-structure turbulence in the wall region of a turbulent boundary layer. *J. Fluid Mech.* **67**, 125.

WEI, T. & WILLMARTH, W. W. 1989 Reynolds-number effects on the structure of a turbulent channel flow. *J. Fluid Mech.* **204**, 57.